The Pennsylvania State University

The Graduate School

Department of Mechanical and Nuclear Engineering

USING KALMAN FILTERING TO IMPROVE A LOW-COST GPS-BASED COLLISION WARNING SYSTEM FOR VEHICLE CONVOYS

A Thesis in

Mechanical Engineering

by

Stephen M. Chaves

Submitted in Partial Fulfillment
of the Requirements
for the Degree of

Master of Science

May 2010

The thesis of Stephen Chaves was reviewed and approved* by the following:

Sean N. Brennan
Assistant Professor of Mechanical Engineering
Thesis Advisor

H. J. Sommer III
Professor of Mechanical Engineering
Thesis Reader

Karen A. Thole
Professor of Mechanical Engineering
Department Head of Mechanical and Nuclear Engineering

*Signatures are on file in the Graduate School

Abstract

This thesis addresses the concern of rear-end collisions in vehicle convoys, specifically in military applications. The goal of this thesis is to provide a framework for a low-cost, easily-incorporated collision warning system to be used in vehicle convoys. Such a system can have immediate and substantial impact on saving lives. Military convoys in particular often operate in dusty conditions or adverse weather, and existing radar-based collision detection systems can have degraded performance in these situations. This thesis proposes a collision warning system that is based on a GPS receiver and wireless network for transferring data between convoy vehicles. In order to meet the accuracy requirements outlined by others for successful collision avoidance, this work focuses on improving the vehicle velocity measurements which are not sufficient by themselves. The GPS receiver measurements are fused with readings from a MEMS accelerometer in a Kalman filter. The Kalman filter greatly increases the performance of the proposed collision warning system with only a slight increase in cost. The results of this thesis show that with this type of data fusion, a low-cost GPS-based collision warning system is both feasible in terms of meeting accuracy requirements of collision avoidance systems, and realizable by demonstration through numerous field experiments conducted as part of this thesis.

Table of Contents

List of Figures

List of Tables

Acknowledgments

I would first like to thank my thesis advisor, Dr. Sean Brennan, for working with me since before my graduate research even began. Thank you for your guidance, teaching, and support throughout my years in your research group. It has been a pleasure to learn under you and work as your student.

Thank you to Penn State Applied Research Laboratory and Army TACOM for support on this project and providing the funding and direction for this research.

Thank you to the members of the Intelligent Vehicles and Systems Group for help with my research and making the day-to-day life in the lab fun. Thanks to Sanket Amin for working with me on the collision avoidance research project that led to most of the work presented in this thesis.

Thanks to the Department of Mechanical and Nuclear Engineering and Penn State University for a very enjoyable undergraduate and graduate career. Many thanks to the Department of Defense SMART Scholarship Program for supporting me during my last year in school.

Thank you to my parents, family, and friends who have always supported my decisions and encouraged my endeavors. A special thank you to my fiancée Allison for all the love that you give to me. I cannot wait to begin my life with you.

Most importantly, I am eternally grateful to my Lord Jesus Christ, for whom I work (Colossians 3:17, 23). None of my earthly accomplishments can ever compare to the wisdom, hope, fulfillment, and salvation found in You (1 Corinthians 1:30).

To my beautiful and loving future wife

Allison

Chapter 1

Introduction

This thesis addresses the concern of rear-end collisions in vehicle convoys. While the focus of this work is specifically in military applications, the results apply also to future commercial vehicles with modest and expected advances in technology. The goal of this thesis is to provide a framework for a low-cost, easily-incorporated collision warning system to be used in vehicle convoys. Such a system can have immediate and substantial impact on saving lives.

1.1 Motivation

There are many situations – in particular military scenarios, automated highways, etc – where vehicles must operate in convoys wherein several vehicles follow the same path in single line formation or "column". When humans are operating vehicles in close proximity, there is a grave concern about possible accidents, particularly rear-end collisions, as driving habits of individual drivers vary.

1.1.1 Commercial Sector

This concern is reflected in the commercial vehicle sector where, according to NHTSA, more than 28% of all vehicle crashes are rear-end collisions, of which more than 60% can be at least partly attributed to driver inattention [**1**]. Driver inattention was shown to be the most influential factor in these rear-end crashes, implying that some sort of detection system could significantly

reduce the number of collisions. Some studies show that the number of collisions could be reduced between 50 and 90% with an additional one second of warning [**2**].

1.1.2 Military Sector

In the military sector, rear-end collisions in convoys are a prevalent concern, especially in domestic training centers. Many rear-end collisions result from low-visibility conditions caused by dust, and occur among young drivers who are unfamiliar with operating heavy trucks in a convoy formation.

The specific focus on convoy operations greatly simplifies the collision detection analysis: the primary focus of this work is on distance keeping between vehicles and not lateral guidance or merge/departure from the convoy. Further, the set of vehicles in the convoy and their ordering is assumed to be constant, and it is assumed that the same path is followed by all vehicles in the convoy. But even with these assumptions, there are obvious situations where Commercial Off-The-Shelf (COTS) solutions are not applicable. Many collision detection systems rely on radar and line-of-sight between vehicles. However, there are many convoy operation scenarios – a military convoy driving in dusty desert conditions, for example – where radar may not be ideal.

Currently, there is interest from the military in researching non-radar-based collision detection systems and passive systems that do not assume vehicle control. Thus, there is motivation to develop an alternative system that adequately warns of rear-end collisions among convoys in dusty conditions. A system that is inexpensive and quickly and easily installed on existing convoy vehicles is desired in order to implement collision warnings as soon as possible.

1.2 Thesis Outline

The subsequent chapters of this thesis are organized as follows:

Chapter 2 presents a literature review of previous research done in the area of collision avoidance algorithms and the necessary requirements for a successful collision avoidance system. Existing commercial systems are examined as well.

Chapter 3 gives an introduction to Global Positioning System (GPS) and its functionality. The collision warning system proposed in this thesis relies on GPS measurements, so knowledge of how GPS operates is beneficial.

Chapter 4 outlines the collision warning system that is proposed to address the problem of rear-end collisions in military vehicle convoys. The concept of the proposed system is presented, along with its theory of operation and intended advantages over existing systems. The chapter concludes with the construction of a prototype system to use for field testing.

Chapter 5 presents initial field tests that were performed with the prototype collision warning system. The performance of the prototype system is assessed with sudden braking events that resulting in a safe stop and a rear-end collision between two vehicles. Basic conclusions on the concept feasibility are given.

Chapter 6 gives background on the Kalman filtering equations that are implemented with the proposed collision warning system in Chapter 7. The framework for a discrete time Kalman filter

is presented. This chapter also provides a discussion on the characterization of the sensor errors that are applicable to the prototype system.

Chapter 7 discusses the implementation of the Kalman filter with the prototype collision warning system. Data collection and field testing to analyze the Kalman filter performance is outlined, as well as the refinement of the Kalman filter based on the results from these tests.

Chapter 8 is a summary of the results from initial field testing and Kalman filter implementation. A general analysis of the prototype system performance is presented, specifically with respect to the velocity estimate from the Kalman filter and its influence on the proposed collision warning algorithm. The general trend in system performance vs. cost is analyzed based on the results from the prototype system.

Chapter 9 outlines the conclusions from the thesis and presents the future work that follows from the development of the proposed collision warning system.

Chapter 2

Literature Review of Previous Research

Since the early 1990's, collision detection has been a goal in the area of vehicle automation and driver assist, motivated highly by the statistics of crashes in the commercial sector. Automotive companies were the first to research collision warning systems. Doi, et al. from Mazda R&D indentified four main technological components that are necessary for successful collision avoidance, and that must be included in a collision avoidance system [**3**]. These four components are as follows: 1) driving environment detection, 2) path estimation algorithm, 3) safe/danger decision algorithm, and 4) longitudinal automatic brake control. For this thesis, the fourth component will be redefined as 'warning or intervention,' as this category encompasses both passive and active collision avoidance systems considered hereafter. Passive systems are simply just collision *warning* systems, where the driver always has complete control of the vehicle. An active system can be defined as a collision *avoidance* system, where the system assumes control of the vehicle when a collision is detected and the driver fails to respond.

The first component outlined above, driving environment detection, is accomplished in most commercial collision detection systems by scanning laser radar or millimeter wavelength radar. Many other sensor suites have been used, however, including sonar, machine vision, video cameras, infrared sensors, and lasers [**4**].

Regardless of the detection method, there are minimum requirements for driving environment detection in order to adequately sense the surroundings to accomplish successful collision avoidance. For example, Kamiya, et al. of Honda outlined minimum specifications which are given in Table 2.1 [**5**]. Note that these detection specifications extend from the front and center of a vehicle, and were developed with a forward-mounted radar system in mind.

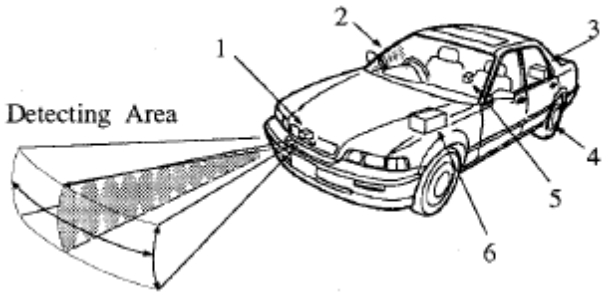

Figure 2.1. Illustration of the driving environment detecting area (From Kamiya, et al. [5**])**

Table 2.1. Minimum driving environment detection specifications as outlined by Kamiya, et al. [5**]**

Description	Specification
Longitudinal detecting range	≥ 100 m
Horizontal detecting area	≥ 350 mrad
Vertical detecting area	≥ 50 mrad
Horizontal resolution	≤ 5 mrad
Range accuracy	≤ 1 m
Refresh time	≤ 0.1 s

The next key component is a path estimation algorithm, which estimates the radius of curvature of the host vehicle's path to better determine whether any obstacles or other vehicles lay in that path. The first collision avoidance systems worked only on straight roads [**3**]. Later work by

Doi, et al. presented simple vehicle dynamics equations for calculating the radius of curvature of a vehicle's path from measured steering input or vehicle yaw rate. The necessity for finding the vehicle's projected path is displayed by Figure 2.2. These equations are not presented because it will be seen later that the convoy driving situation allows for a new method to determine a vehicle's path – by following GPS waypoints from preceding vehicles.

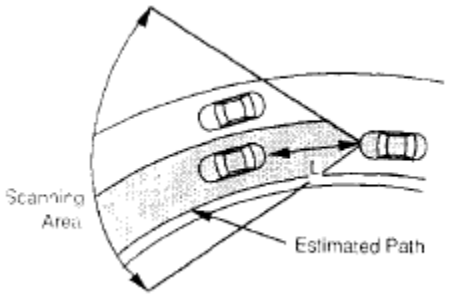

Figure 2.2. Illustration of the estimated path around a curved roadway (From Doi, et al. [3])

The third component, the safe/danger decision algorithm, generally follows a simple physical derivation of two decelerating vehicles. The safe/danger decision algorithm compares the current spacing between the two vehicles (from the driving environment detection) to the spacing needed for each vehicle to come to a complete stop. This necessary stopping distance is called the critical distance. The critical distance definition given by Doi, et al. from Mazda is shown in Equation (2.1), where v is the host vehicle's velocity, v_{rel} is the relative velocity between the host vehicle and preceding vehicle, α_h is the maximum deceleration of the host vehicle, α_p is the maximum deceleration of the preceding vehicle, τ_1 is the deceleration time, τ_2 is the delay time, and d_0 is the buffer distance between vehicles:

$$d_{critical} = \frac{1}{2}\left(\frac{v^2}{\alpha_h} - \frac{(v - v_{rel})^2}{\alpha_p}\right) + v\tau_1 + v_{rel}\tau_2 + d_0 \qquad (2.1)$$

The maximum decelerations, time delay, and distance buffer are all tunable parameters that are adjusted depending on the current driving conditions and driver preference. The collision avoidance system engages when the current headway distance becomes less than the critical distance. This algorithm is an example of a conservative system because it will attempt to avoid all detected rear-end collisions within a convoy of vehicles. Collision avoidance using steering and braking is more difficult than using a braking maneuver – steering inputs can result in possible loss of braking forces – so a conservative system may apply the brakes on the vehicle only well in advance of where someone may be able to swerve to avoid the collision. A non-conservative system waits to apply the brakes assuming the driver may input a corrective steering maneuver. The tradeoff, of course, is that the system may not be able to prevent an impending collision if the driver does not steer appropriately.

Researchers from Honda decided to use a less conservative critical distance definition, shown in Equation (2.2) [**6**]. In this equation, v_h is the host vehicle's velocity, v_p is the preceding vehicle's velocity, v_{rel} is the relative velocity between the vehicles, α_h is the maximum deceleration of the host vehicle, α_p is the maximum deceleration of the preceding vehicle, τ_1 is the system delay time (set to 0.5 s), and τ_2 is the braking time (set to 1.5 s).

$$d_{critical} = \begin{cases} \tau_2 v_{rel} + \tau_1 \tau_2 \alpha_h - 0.5\alpha_1 \tau_1^2 & \frac{v_p}{\alpha_p} \geq \tau_2 \\ \tau_2 v_h - 0.5\alpha_1 (\tau_2 - \tau_1)^2 - \frac{v_p^2}{2\alpha_p} & \frac{v_p}{\alpha_p} < \tau_2 \end{cases} \quad (2.2)$$

In 1998, as part of the California PATH initiative, Seiler, et al. refined the traditional safe/danger decision algorithm in an attempt to increase performance for passive and aggressive drivers and for all road conditions [**7**]. This was achieved by outlining an algorithm that used a conservative

warning critical distance and a non-conservative braking critical distance. In other words, the proposed system would warn the driver of an impending collision early, giving the driver time to react. Then, if the driver failed to react even with a steering maneuver, the system would begin automatic braking. The Mazda algorithm (Equation (2.1)) was modified to serve as the warning critical distance, given in Equation (2.3). The non-conservative braking critical distance is given in Equation (2.4).

$$d_{warn} = \frac{1}{2}\left(\frac{v^2}{\alpha} - \frac{(v - v_{rel})^2}{\alpha}\right) + v\tau + d_0 \tag{2.3}$$

$$d_{brake} = v_{rel}\left(\tau_{sys} + \tau_{hum}\right) + 0.5\alpha\left(\tau_{sys} + \tau_{hum}\right)^2 \tag{2.4}$$

Seiler, et al. also made contributions to the warning or intervention component of collision detection systems by introducing a non-dimensional warning parameter to alert drivers effectively [**7**]. The warning parameter, *w*, shown in Equation (2.5), is simply calculated as the ratio of the current headway distance between the vehicles, *d*, minus the braking distance to the warning distance minus braking distance.

$$w = \frac{d - d_{brake}}{d_{warn} - d_{brake}} \tag{2.5}$$

If the value of the warning parameter is greater than or equal to one, the current driving situation is considered safe. Values between one and zero constitute unsafe conditions and different warnings are provided to the driver. The system assumes control and begins to brake when the warning parameter reaches a value of zero. Seiler, et al. also proposed the addition of a friction factor and driver tuning factor to scale the critical distance [**7**]. The friction factor, $f(\mu)$, is given

in Equation (2.6). In this equation, μ is the tire-road friction coefficient and the other variables are tunable based on the current driving situation.

$$f(\mu) = f(\mu_{min}) + \frac{f(\mu_{norm}) - f(\mu_{min})}{\mu_{norm} - \mu_{min}}(\mu - \mu_{min}) \tag{2.6}$$

The driver tuning factor is set to a default value of 1 to represent no bias in driver preference. Both the warning and braking critical distances are scaled by multiplying them by the friction factor and driver tuning value, as shown in Equations (2.7) and (2.8), to account for the current tire-road friction coefficient and driver preference. The warning parameter is then updated accordingly.

$$d_{warn\ ,scaled} = d_{warn} * f(\mu) * g(driver) \tag{2.7}$$

$$d_{brake\ ,scaled} = d_{brake} * f(\mu) * g(driver) \tag{2.8}$$

2.1 Evaluation of Collision Detection Algorithms

By the 2000's, much research had been done on the development of collision detection algorithms. In 2005, Lee and Peng published a comparison of different algorithms and evaluated their performance with regard to the tradeoff between false alarms and missed detections (the same tradeoff between conservative and non-conservative systems) [**8**]. This performance evaluation incorporated human perceptions and varying human characteristics for a range of driving situations. Hoffman and Mortimer asserted that the time-to-collision (TTC) metric is the most direct measure of a driver's perception of the risk of a rear-end collision [**9**] and should thus be used to determine the effectiveness of a collision prediction from a collision warning algorithm. The time-to-collision metric is given in Equation (2.9), where *d* is the current

headway distance, v_{rel} is the relative velocity between vehicles, and β is the visual angle subtended by the preceding vehicle to the driver of the host vehicle.

$$TTC = d/v_{rel} = \beta/(d\beta/dt) \tag{2.9}$$

In most cases, drivers underestimate the TTC, meaning they tend to avoid collisions by braking more aggressively than necessary because they perceive the collisions to be more imminent than they are in reality. Lee and Peng showed that the TTC metric performed well in accurately distinguishing safe and threatening driving situations – better than the collision detection algorithms that were studied. Thus, they claim that there is much room for collision detection algorithm improvement. Most algorithms are designed to reduce false alarms but suffer from missed detections and may, at times, fail to provide warnings in a timely manner [**8**]. Algorithms that could better estimate the TTC could better predict actual rear-end collision scenarios. Shladover and Tan stated that estimates of TTC from collision detection systems should be within 200 to 500 ms of the actual TTC since this slight error would likely go undetected by humans [**10**]. This requirement would ensure a timely delivery of a warning issued by a system.

2.2 Existing Commercial Systems

There are many commercial-off-the-shelf (COTS) collision detection systems that exist today, most of which are used in the trucking and public transportation industries. Eaton [**11**], Delphi [**12**], and Meritor Wabco [**13**] developed systems that use forward-looking radar to scan for vehicles and obstacles in the host vehicle's path of travel. They are all active collision avoidance systems that will automatically brake the vehicle if necessary. Mobileye produces a system that is CMOS camera-based [**14**], and Siemens VDO combines LIDAR and CMOS cameras to warn

of lane departures and possible rear-end collisions ahead [**15**]. Almost all commercially-available collision detection systems have adaptive cruise control (ACC) or safe distance-keeping capability, where the system automatically adjusts the speed of the vehicle's cruise control if it senses the headway distance is decreasing. Hence, these systems are usually marketed as "driver assistance systems" because they have a range of capabilities extending beyond collision detection.

By far, the most well-known and most widely-used collision avoidance system is the Bendix VORAD (recently sold to Bendix by Eaton), common on trucking fleets and heavy military vehicles. Their newest model, the VORAD VS-400, features a 77 GHz forward looking radar mounted front and center on the host vehicle's bumper [**11**]. This radar has an operating range of 3 to 500 feet and 0.5 to 120 mph and is able to track up to 20 vehicles simultaneously. VORAD also includes a side object detection system called BlindSpotter that alerts drivers when an object is detected alongside the vehicle. The Driver Interface Unit serves as the warning system inside the cab of the truck, providing the driver with audible signals and warning lights, and can display time-to-collision projections and fault indicators.

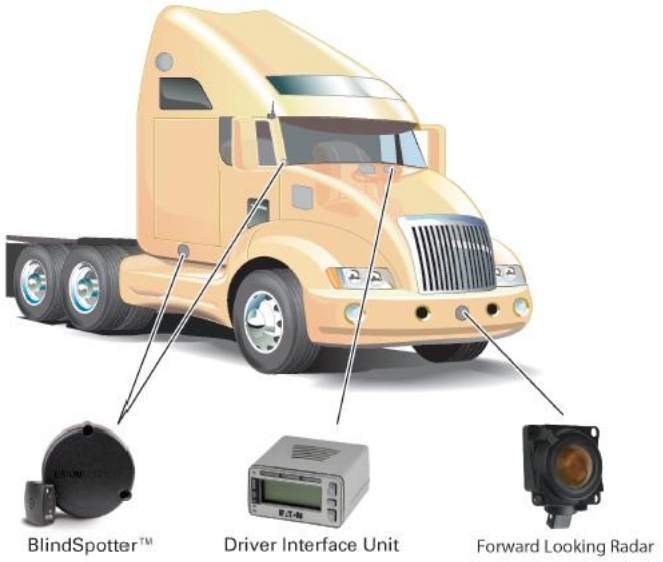

Figure 2.3. Overview of VORAD VS-400 (From Eaton Corporation [16**])**

2.2.1 Limitations of Radar-Based Systems

While these systems meet all of the necessary requirements for successful environment detection given in Table 2.1, they tend to be expensive [**10**] and leave much to be desired in terms of performance and driver acceptance. Collision avoidance systems reliant on radar measurements will be restricted by inherent limitations of radar and how it senses the surrounding environment.

For example, in 2004 Volvo published a report on VORAD that revealed responses from truck drivers interviewed about the system [**17**]. Only 48% of drivers stated that VORAD was helpful when driving on an open highway and 37% of drivers said that VORAD was distracting in heavy-traffic scenarios. They also classified nearly half of the warnings from VORAD as false-positives. Additional complaints were related to a high false alarm rate, distracting audible beeps, and degraded performance when the sensor became blocked from mud or ice.

Davies noted similar performance issues with radar-based systems, stating high false alarm rates are common in situations where the line-of-sight extends beyond the vehicle's path. Since radar has the inability to distinguish obstacles *near* a path to obstacles *on* a path, construction barrels or trees alongside a roadway will appear to a radar system as a static vehicle. Depending on the accuracy of the path estimation algorithm, objects like construction barrels will trigger the system to warn of a collision, even when the driver will successfully navigate around the barrels. This response will significantly increase the number of false-positive alarms and decrease driver acceptance.

Radar systems do not work in non-line-of-sight conditions either, as they are unable to identify objects over hills or around blind bends in the vehicle's path. This limitation makes it very difficult to accurately predict potential collision scenarios in urban environments, winding and wooded landscapes, and hilly terrain. While sighting distance regulations exist for engineered roadways, they do not exist in many areas where convoys are operated, for example military convoys in back-country roads.

Radar is compromised by adverse weather conditions or occluding particles [**18**]. Because radar relies on the reflection of waves off obstacles to determine distance, backscatter from raindrops, dust, or snow can decrease performance precisely during the times when the driver may be most reliant on the warnings provided by the system. Radar systems that are mounted on vehicle bumpers can also experience sensor blockage, due to mud or ice, rendering the radar useless until it is cleaned.

Chapter 3

Introduction to Global Positioning Systems

3.1 Overview of GPS

The Global Positioning System (GPS) was developed by the U.S. Department of Defense (DoD) and first declared fully operational in 1995. Its original objective was to provide the U.S. military with accurate estimates of position (< 10 m error), velocity (< 0.1 m/s error), and time (< 100 ns). GPS was designed to offer two services: Standard Positioning Service (SPS) for civilian use and Precise Positioning Service (PPS) for DoD-authorized use. The SPS service broadcasts on the L1 frequency of 1575.42 MHz and uses a coarse/acquisition code (C/A code). The PPS uses the L1 frequency and the L2 frequency of 1227.60 MHz. The PPS uses an encrypted P(Y) code on the L1 and L2 for more accurate positioning than the SPS.

The GPS system architecture consists of three segments: the space segment, the control segment, and the user segment. Each is necessary for the overall operation of GPS. The space segment is composed of 24 to 32 satellites orbiting the earth at 11,000 miles above the surface. The satellites are arranged on six different planes inclined at 55 degrees relative to the equatorial plane. This way, almost all locations on earth will have at least 4 satellites in view at any time – the minimum number needed to estimate a 3D location and user time bias. As more satellites are added to the baseline constellation, most users are capable of seeing 6 to 8 satellites with a clear view of the

sky. The satellites continuously broadcast ranging signals and navigation data over the L-band frequencies specified above.

The control segment monitors the orbits and maintains the health of the satellites in the GPS constellation. It also maintains GPS time, predicts satellite and clock parameters, and updates the navigation data for each satellite. The Master Control Station (MCS) is located in Colorado Springs, Colorado at Schriever Air Force Base. Numerous other stations are spread out longitudinally across the earth so that each satellite can be monitored by at least two stations at all times.

Lastly, the user segment represents the civilian, commercial, and military users of GPS, made possible by GPS receivers. Receivers range in price from about $50 to many thousands of dollars and have varying capabilities and applications. Since 1997, more than one million GPS receivers have been produced each year. Civilian and commercial use of GPS has grown in the last 10 years, thanks in part to the removal of Selective Availability (SA) in May 2000. Before that time, the C/A code carried on the L1 frequency was purposefully degraded with controlled errors to limit the accuracy of non-DoD user positioning. The elimination of this signal greatly increased the accuracy of the public system after 2000.

3.2 GPS Functionality

Each GPS satellite transmits signals that have three components: the carrier, the ranging code, and the navigation data. The carrier is simply a radio-frequency sinusoidal signal that broadcasts at the L1 and L2 frequencies. The ranging code is a set of Pseudo-Random Noise (PRN) sequences for both the SPS (called C/A code) and PPS (called P(Y) code). The PRN codes are

distinct to each satellite and use a specific type of modulation called binary phase shift keying (BPSK). The C/A code is composed of a 1023-bit sequence repeated each millisecond at a rate of 1.023 MHz. The P(Y) code is a much longer sequence at 10^{14} bits, and repeated at a rate of 10.23 MHz. The P(Y) code is able to yield more accurate range measurements because it has a wavelength of 30 m, as compared to the 300 m wavelength of the C/A code. The navigation data is the last component of a GPS signal. This message contains information regarding satellite health, satellite orbital parameters, clock parameters, and general information about the entire satellite constellation. Each satellite has an onboard 10.23 MHz atomic standard that schedules the transmission of the GPS signals.

3.2.1 Calculating Position

GPS receivers can calculate user position and velocity because they are able to decode the signals from the GPS satellites. Each receiver is capable of producing a replica reference signal for each satellite by duplicating the PRN sequence from that satellite and using BPSK. The receiver then compares the replica reference signal to the signal it actually received. From this comparison, the receiver determines the phase lag between the two signals that represents the transmission time from the satellite, and (when multiplied by the speed of light) calculates a pseudorange measurement to that satellite. The pseudorange from the *k*th satellite at GPS time *t* is given by

$$\rho^{(k)}(t) = r^{(k)}(t, t-\tau) + c\left[\delta t_u(t) - \delta t^{(k)}(t-\tau)\right] + I^{(k)}(t) + T^{(k)}(t) + \varepsilon_\rho^{(k)}(t) \qquad (3.1)$$

where k is the satellite number (k = 1, 2, 3,…, K), $r^{(k)}$ is the actual range between the receiver at reception time t and satellite at transmission time (t-τ), c is the speed of light, δt_u and $\delta t^{(k)}$ are the receiver and satellite clock biases, respectively, I and T are the ionospheric and tropospheric propagation delays, respectively, and ε represents other modeling errors. To save on cost, most

receivers employ an inexpensive quartz crystal oscillator as a timer. Thus, receiver clocks will drift from true GPS time, so the pseudorange measurement includes a significant user time bias.

The pseudorange measurement equation can be rewritten as

$$\rho_c^{(k)} = \sqrt{(x^{(k)} - x)^2 + (y^{(k)} - y)^2 + (z^{(k)} - z)^2} + b + \tilde{\varepsilon}_\rho^{(k)} \tag{3.2}$$

where $x^{(k)}$, $y^{(k)}$, and $z^{(k)}$ are the satellite coordinates in the earth-centered, earth-fixed (ECEF) frame, x, y, and z are the user coordinates in ECEF, b is the user clock bias, and ε accounts for all sources of error. A minimum of four pseudorange measurements are needed for position estimation because there are four unknowns, namely x, y, z, and b. The position solution follows from a standard least-squares estimation problem, where the "best" solution minimizes the sum of the squared residuals. Position accuracy is directly related to the number of satellites in view and their geometry in the sky. The accuracy will most likely increase if more than four pseudorange measurements are available and the satellites are spread out nicely in elevation and azimuth.

3.2.2 Calculating Velocity

Velocity estimation is done using the Doppler shift between the satellite and user. With the satellite velocity known, the Doppler shift (or pseudorange rate) can be found by differentiating the pseudorange measurement from Equation (3.2). The pseudorange rate is given by

$$\dot{\rho}^{(k)} = \left(\mathbf{v}^{(k)} - \mathbf{v}\right) \cdot \mathbf{1}^{(k)} + \dot{b} + \varepsilon_\varphi^{(k)} \tag{3.3}$$

where $\mathbf{v}^{(k)}$ and $\mathbf{v}$ are the satellite and user velocity vectors, respectively, $\mathbf{1}^{(k)}$ is the user-to-satellite unit line-of-sight unit vector, $\dot{b}$ is the rate of change of the receiver clock, and ε accounts for all sources of error. The velocity solution is found once again using least-squares estimation with at least four pseudorange rate measurements.

3.2.3 Measurement Error Sources

Errors in the GPS measurements fall into three categories: control segment errors, signal propagation errors, and receiver measurement errors. The control segment errors are mainly errors in satellite position and clock bias. While orbital prediction algorithms and clock technologies are improving, they are not perfect, and account for 2-3 m in error.

Signal propagation errors can be attributed to propagation delays in the ionosphere and troposphere. The speed of the signal varies as it travels through different atmospheric layers, resulting in a skewed estimate of the range to the satellite. There are models that can predict these propagation delays, reducing the errors to 1-5 m for the ionosphere and 0.1-1 m for the troposphere. A dual-frequency receiver has the benefit of almost fully eliminating the ionospheric error by discriminating the error source from the two measurement signals. This error mitigation is possible because of the dispersive property of the ionosphere where the refractive index is dependent upon the frequency of the signal. The troposphere is a non-dispersive medium, so a dual-frequency receiver has no advantage to reducing tropospheric errors.

The main components of measurement errors are receiver noise and multipath. Receiver noise is random and uncorrelated and generally accounts for less than 0.5 m in error. Multipath occurs when the signal from a satellite is received in a non-line-of-sight manner (i.e. reflecting off

buildings, canyon walls, or the ground). Multipath can be prevented if the receiver is placed away from obstructions, but errors can be up to 5 m in a highly-reflective area.

3.2.4 Differential GPS

Code-based pseudorange measurements acquired by a single GPS receiver can have errors up to 6 m, translating to a position solution with horizontal errors up to 10 m. The control segment errors and propagation errors are highly correlated both spatially and temporally. Since these errors change slowly in time and are similar for receivers within tens of kilometers of each other, greater positioning accuracy can be gained with a differential GPS (DGPS) system. DGPS utilizes these correlations to almost completely eliminate errors from satellite position, clock bias, and propagation delays.

DGPS functions on the idea that a stationary receiver is placed at a known location and the effect of the errors can be determined for this receiver. Then, the error estimates are broadcast to nearby receivers in order to improve their own measurements. With DGPS, the horizontal error of a position solution is reduced from a possible 10 m to 1 m.

3.3 Transformation of Coordinates

To understand how GPS calculates a user position on the earth, it is necessary to review coordinate conversions that are used. Satellite navigation data is given in an ECEF coordinate frame, so it is convenient to calculate user position in the ECEF frame. However, this frame is not very helpful when trying to understand how a point on this frame relates spatially to the surface of the earth. Thus, more convenient frames are used: a geodetic frame (ellipsoidal coordinates) with coordinates of latitude, longitude, and altitude (LLA), and a Cartesian frame

with origin on the surface of the earth and horizontal axes oriented along the east and north directions and a vertical axis pointed up (ENU). From this point on, these frames will be called LLA and ENU, respectively.

Additionally, GPS uses a set of fundamental parameters called World Geodetic System 1984 (WGS 84) that is the official reference for all DoD-related mapping and navigation. WGS 84 outlines the ECEF coordinate frame used by GPS, characterizes the earth's revolution and gravitational field, and provides a standard for important constants. Table 3.1 provides parameters that are necessary for the coordinate conversions below.

Table 3.1. WGS 84 fundamental parameters (revised in 1997) [19**]**

Parameter	Value
Ellipsoid semi-major axis (a)	6378137.0 m
Ellipsoid semi-minor axis (b)	6356752.3142 m
Ellipsoid reciprocal flattening ($1/f$)	298.257223563
Earth's first eccentricity (e)	0.081819190842621
Earth's angular velocity (ω_E)	7292115.0e-11 rad/sec
Earth's gravitational constant (GM)	3986004.418e8 m^3/s^2
Speed of light in a vacuum (c)	2.99792458e8 m/s

3.3.1 Conversion between ECEF and LLA

The transformation from ECEF (x, y, z) to LLA (ϕ, λ, h) is an iterative process that begins with finding the longitude, λ.

$$\tan(\lambda) = {}^{y}/_{x} \tag{3.4}$$

The rest of the transformation is made easier with some other definitions, the distances *N* and *p*.

$$N = \frac{a^2}{(a^2 \cos^2 \phi + b^2 \sin^2 \phi)^{1/2}} = \frac{a}{(1 - e^2 \sin^2 \phi)^{1/2}} \tag{3.5}$$

$$p = \sqrt{x^2 + y^2} = (N + h) \cos \phi \tag{3.6}$$

Then, the altitude, *h*, is given by

$$h = \frac{p}{\cos \phi} - N \tag{3.7}$$

and the latitude, ϕ, is given by

$$\tan \phi = \frac{z}{p}\left(1 - e^2 \frac{N}{N + h}\right)^{-1} \tag{3.8}$$

So, after calculating the longitude from Equation (3.4), the latitude and altitude are found by iterating between Equations (3.7) and (3.8).

The transformation from LLA to ECEF is more direct, and is given in Equation (3.9) below.

$$\begin{bmatrix} x \\ y \\ z \end{bmatrix} = \begin{bmatrix} (N + h) \cos \phi \cos \lambda \\ (N + h) \cos \phi \sin \lambda \\ (N(1 - e^2) + h) \sin \phi \end{bmatrix} \tag{3.9}$$

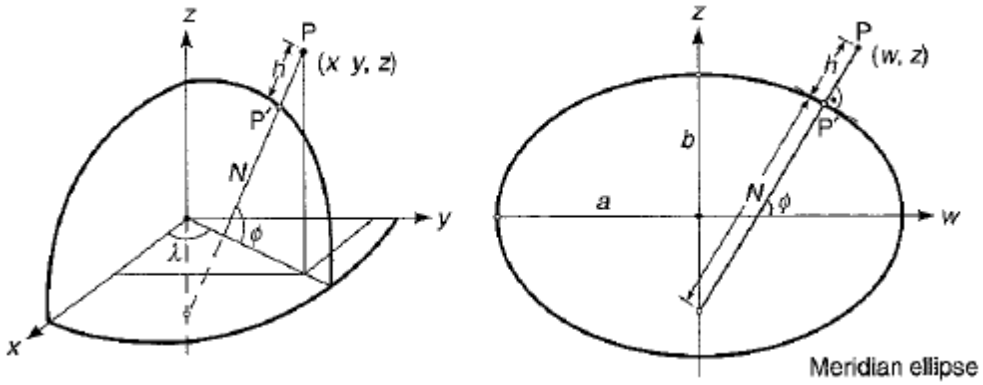

Figure 3.1. Cartesian ECEF and geodetic LLA coordinate frames (From Misra and Enge [20])

3.3.2 Conversion between ECEF and ENU

The transformation from ECEF (x, y, z) to ENU (x_E, x_N, x_U) requires a reference point expressed in ECEF, which will be denoted by (x_R, y_R, z_R), and which will serve as the origin of the ENU frame. The elementary rotations that bring the ECEF frame into coincidence with the ENU frame are given in Equation (3.10) and use the geodetic latitude and longitude from the LLA frame.

$$\mathbf{R}_L = \begin{bmatrix} -\sin\lambda & \cos\lambda & 0 \\ -\sin\phi\cos\lambda & -\sin\phi\sin\lambda & \cos\phi \\ \cos\phi\cos\lambda & \cos\phi\sin\lambda & \sin\phi \end{bmatrix} \tag{3.10}$$

Then, the transformation from ECEF to ENU is given by

$$\begin{bmatrix} x_E \\ x_N \\ x_U \end{bmatrix} = \mathbf{R}_L \begin{bmatrix} x - x_R \\ y - y_R \\ z - z_R \end{bmatrix} \tag{3.11}$$

The transformation from ENU to ECEF is given by

$$\begin{bmatrix} x \\ y \\ z \end{bmatrix} = \mathbf{R}_L^T \begin{bmatrix} x_E \\ x_N \\ x_U \end{bmatrix} + \begin{bmatrix} x_R \\ y_R \\ z_R \end{bmatrix} \tag{3.12}$$

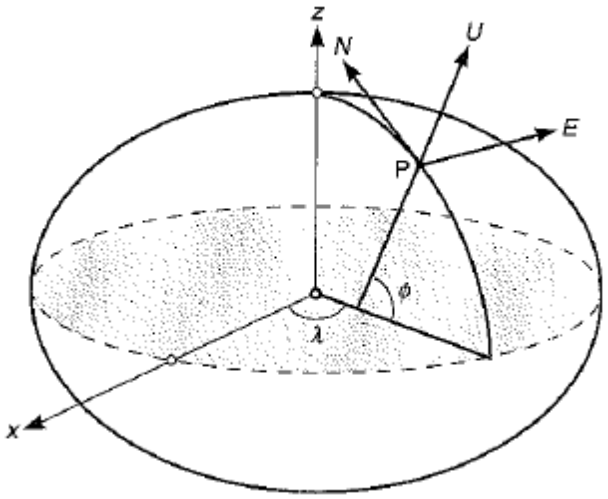

Figure 3.2. The East-North-Up (ENU) coordinate frame (From Misra and Enge [20**])**

Chapter 4

The Proposed Collision Warning System

This thesis is motivated by the problem of rear-end collisions in military vehicle convoys. Based on the review of existing research on collision detection systems, a set of design criteria was established to guide the development of a new collision detection system. The design criteria are as follows:

- The system must be accepted by a wide variety of drivers.
- The system must perform well in all driving situations and weather conditions.
- The system must adequately alert the driver of an impending rear-end collision.
- The system must accurately distinguish between safe and unsafe driving situations.
- The system must be inexpensive and easily incorporated onto existing convoy vehicles.

It was determined that, for this problem and application, the driving environment detection would be best accomplished by focusing on detecting the other vehicles in the convoy. Although radar is commonly used, an alternative method is desired based on the limitations discussed in the previous chapters. Currently, one of the most common and inexpensive methods to measure vehicle position is by GPS. Commercial GPS receivers are becoming increasingly popular for vehicle applications, including turn-by-turn navigation, fleet monitoring, route recording, and

vehicle dynamics studies. With a GPS unit installed on each vehicle in the convoy, each vehicle's position, velocity, and heading can be continuously reported for driving environment detection.

Before the proposed collision warning system is presented, a number of reasonable assumptions must be outlined to define the scope of the system. The assumptions are as follows:

- All vehicles of interest will be equipped with the proposed collision warning system. No vehicles are present without the system installed.
- All vehicles of interest fit the tunable parameters of the collision warning algorithm or the parameters of the algorithm have been adjusted accordingly.
- There is open-sky visibility in all areas where the system will be used. It is assumed that GPS signals are readily available and not blocked.
- All vehicles of interest are driving in a convoy formation where there are no vehicles entering and exiting the convoy.
- There are no threats of intersection collisions, collisions on the side of the vehicle, or collisions with other objects. Only rear-end collisions of convoy vehicles with other convoy vehicles are of interest.

These are all easy assumptions to make with knowledge of the problem at hand, standard convoy specifications, and the current status of sensor technologies.

4.1 Overview of the Proposed GPS-based System

Following the design criteria outlined above, a new collision warning system is now proposed. The proposed system has five main components: a GPS receiver, an accelerometer, a wireless network access point, a computer to process the collision detection algorithm, and a driver display for providing feedback. Each vehicle in a convoy will be equipped with the proposed collision warning system because the overall system requires that all vehicles work together to ensure proper operation. Hence, this type of system is often called a *cooperative* collision warning system [**10**]. Figure 4.1 conceptually illustrates the system.

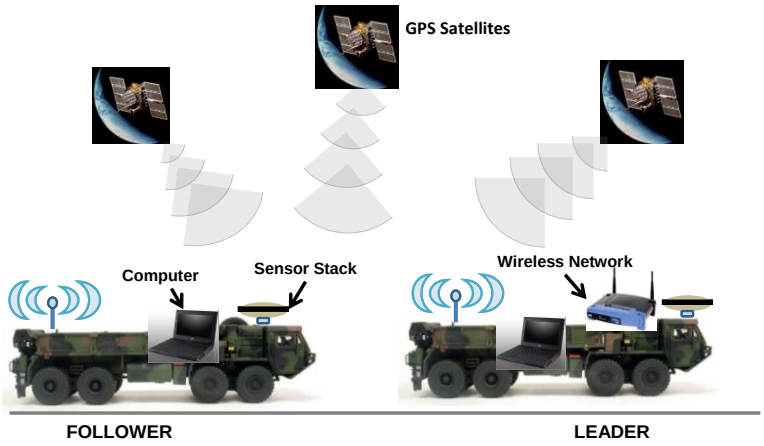

Figure 4.1. Conceptual illustration of the proposed GPS-based collision detection system

4.1.1 GPS Receiver/Accelerometer

A low-cost GPS receiver is the foundation of the proposed collision warning system. The purpose of the GPS receiver is to collect the host vehicle's position, velocity, and heading so this information can be used in the collision warning algorithm. A low-cost MEMS accelerometer complements the GPS receiver and together they comprise the sensor suite necessary for adequate driving environment detection. The accelerometer provides quick updates of the host vehicle's

acceleration and braking events which can be integrated to provide an estimate of the host vehicle's velocity. Unlike the accelerometer, low-cost GPS receivers generally do not provide updates more frequently than a few times each second.

Not only is the GPS and accelerometer information valuable to the host vehicle, but it can be shared among the other convoy vehicles. With each vehicle in the convoy equipped with this sensor suite, each vehicle's position, velocity, acceleration and heading information can be continuously reported to the rest of the convoy. Hence, all convoy vehicles will have knowledge of all the other vehicles in the convoy, allowing the prediction and prevention of rear-end collisions.

4.1.2 Wireless Vehicle Network

A wireless vehicle network is necessary in order to share the GPS information among the convoy vehicles. This network represents a growing concept called Vehicle-to-Vehicle (V2V) communications. Chen and Cai identified that V2V communications must be researched to improve upon the performance of existing collision avoidance systems [**21**]. V2V systems are being considered in commercial vehicle fleets, and are already being developed and deployed in military environments where they can aid in the notification of breakdowns and attacks [**22**]. A particular advance in the last several years is the commercial-off-the-shelf availability of vehicle mesh networks, where high-bandwidth vehicle-to-vehicle communication is readily obtained. For most mesh systems, the vehicle network range (often measured in miles) is not a pressing issue because any rear-end collisions will obviously occur when the wireless network is within a short, reachable range.

4.1.3 Computer

The computer acquires the host vehicle's GPS and accelerometer information and exchanges it with remote computers onboard other convoy vehicles via the wireless network. It is responsible for managing the transmission of data to and from the host vehicle, but it also serves as the processor for the collision warning algorithm. It uses the local and remote vehicle information to calculate the warning parameter that serves as a collision warning indication. While each vehicle shares its own information among the entire convoy, it only calculates a collision warning to the preceding vehicle in the formation.

4.1.4 Driver Display

The driver display continuously provides visual warnings to the host vehicle operator. The warnings are a result of the collision warning algorithm, and they reflect the current driving situation and corresponding chance of collision. Depending on the vehicle and typical driving environment, the driver display may include audible alerts that supplement the visual warnings.

The effectiveness of driving warnings and warning methods are not studied in this thesis, as they introduce more uncertainty and are subject to human variability. Rather, with regard to driver warnings, the research in this thesis is concerned with the timeliness and correctness of a collision warning.

4.2 The Proposed Collision Warning Algorithm

As stated in the previous chapter, a successful collision detection system has four elements, namely driving environment detection, path estimation algorithm, safe/danger decision algorithm, and warning or intervention. The driving environment detection for each vehicle is accomplished

with the sensor suite composed of the GPS receiver and MEMS accelerometer. The warning element is accomplished with the driver display.

4.2.1 The Safe/Danger Decision Algorithm

The safe/danger decision algorithm for the proposed system is based on the algorithm presented by Seiler, et al. in [7] and given in Equations (2.3) – (2.5). Since the proposed system is only a passive collision *warning* system, there is no need to define a critical braking distance. Instead, only the critical warning distance – the distance the vehicles must maintain between each other assuming the most aggressive braking of the lead vehicle – is needed. It is rewritten below.

$$d_{warn} = \frac{1}{2}\left(\frac{v^2}{\alpha} - \frac{(v - v_{rel})^2}{\alpha}\right) + v\tau + d_0 \tag{4.1}$$

Without the critical braking distance, the warning parameter is also modified for use with the proposed system. The warning parameter becomes

$$w = \frac{d}{d_{warn}} \tag{4.2}$$

In this case, if the value of the warning parameter is greater than or equal to one, the current driving situation is considered safe. Once the warning parameter reaches a value of zero, though, the current headway distance has completely eclipsed to zero, implying a collision has occurred. Thus, values between one and zero constitute unsafe conditions. As the value approaches zero, the severity of the warning increases.

The proposed system algorithm adopts the scaling of the critical warning distance using the friction factor and driver tuning factor, as shown in Equations (2.6) – (2.8). The modified warning parameter (Equation (4.2)) is then updated accordingly.

4.2.2 Calculation of the Headway Distance

Most existing systems, like those that use radar for driving environment detection, can directly measure the headway distance between two vehicles. In the case of the proposed system that uses GPS, the headway distance must be derived from the positions of the vehicles. The haversine formula is used to find this distance [**23**]. Assuming a spherical earth with radius *R* equal to 6371 km, this formula yields the great-circle distance between two sets of latitude and longitude points. Altitude is neglected. Refer to Equations (4.3) – (4.7) for pseudocode of the haversine formula.

$$\Delta lat = latitude_1 - latitude_2 \tag{4.3}$$

$$\Delta lon = longitude_1 - longitude_2 \tag{4.4}$$

$$a = \sin^2\left(\frac{\Delta lat}{2}\right) + \cos(latitude_1) * \cos(latitude_2) * \sin^2\left(\frac{\Delta lon}{2}\right) \tag{4.5}$$

$$c = 2 * \sin^{-1}\left(\min(1, \sqrt{a})\right) \tag{4.6}$$

$$distance = R * c \tag{4.7}$$

4.3 Advantages of the Proposed System

A GPS-V2V based collision avoidance system has many potential advantages over traditional radar-based systems, including desirable performance in each of the areas where the radar system fails, described previously. These advantages are presented below.

4.3.1 Non-Line-of-Sight Operation

Because the GPS system uses a wireless network to communicate information, the GPS system has non-line-of-sight capabilities. Unlike the radar system, the GPS system is able to detect other vehicles over hills and around bends.

4.3.2 Better Performance in Inclement Weather

The GPS system also has better performance than the radar system in adverse weather conditions. Military and commercial wireless vehicle networks (V2V communications) are designed to be robust to weather and should continue to transmit data between vehicles in times of heavy precipitation or dust. This would mitigate the erroneous measurement problems characteristic of radar systems affected by backscatter.

4.3.3 Path Estimation and Improved Obstacle Detection

The specific nature of the problem – convoy collision detection – also allows for this GPS-based system to take a unique approach to the path estimation algorithm. For each vehicle in the convoy that is not the lead vehicle, the estimated path can be assumed to be the same path that was traversed by the preceding vehicle. The GPS-waypoint path outlined by the lead vehicle is continually refined by each following vehicle. The focus for obstacle detection is then only necessary in this previously swept envelope and roadside objects along the path can be ignored, as depicted in Figure 4.2. Rear-end collisions only need to be detected on a one-dimensional pathway.

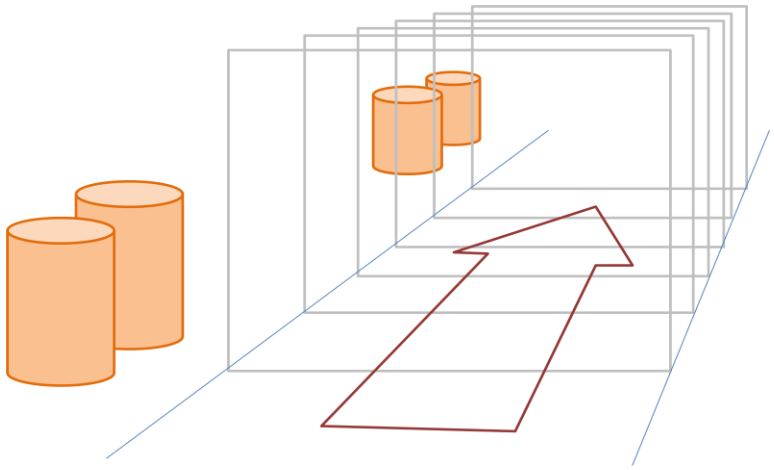

Figure 4.2. The projected pathway for a vehicle, as given by GPS waypoints from preceding vehicles in a convoy

4.4 Construction of the Prototype

To test the concept of the proposed collision detection system, prototype systems were constructed. Since the GPS receiver is the foundation of the proposed collision warning system, much testing was performed to select the low-cost receiver best suited for the application. Most low-cost receivers provide updates at 1 Hz or less. This frequency was found to be very undesirable as a vehicle's position and velocity are able to change drastically during the one second between consecutive GPS measurements. A collision warning system must provide warnings on time, so a faster update rate is desirable.

The low-cost GPS receiver that was selected is the San Jose Navigation FV-M8, available for $100. It features a 5 Hz update rate and accepts standard DGPS correction protocols. See Figure 4.3 for a view of this receiver.

Figure 4.3. San Jose Navigation FV-M8 GPS receiver (From Sparkfun.com)

The MEMS accelerometer chosen for the prototype system is the ADXL 335 from Analog Devices, available for $25. It is a three-axis accelerometer with a sensing range of +/- 3g on each axis. See Figure 4.4 for a view of this accelerometer.

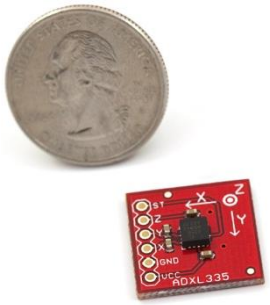

Figure 4.4. Analog Devices ADXL 335 triple axis accelerometer (From Sparkfun.com)

An Arduino Mega microcontroller ($60) parses the data from the GPS and accelerometer before sending it over Ethernet to the computer. Together, the GPS, accelerometer, and microcontroller form the sensor suite described in Section 4.1.1 for the prototype system. These components were placed in a clear waterproof case and mounted to a metal plate with magnetic feet. This unit is called a "sensor box," and is easily attached to the roof of a vehicle. A cooling system consisting of a PC fan and aluminum foil shielding was installed in the sensor box to prevent

overheating of the electronics during field testing. Overheating can especially be an issue in many desert environments where convoys often operate.

The computer used by the prototype system is a Dell Latitude 2100 equipped with MATLAB/Simulink and real-time control software called QuaRC. The computer receives the sensor data from the microcontroller over Ethernet and transmits it back out over the wireless vehicle network. The prototype system uses an 802.11 Ad Hoc network to share data among vehicles, aided by network extenders also mounted in the sensor boxes. The computer associated with each sensor box processes the collision warning algorithm and displays the driver warning.

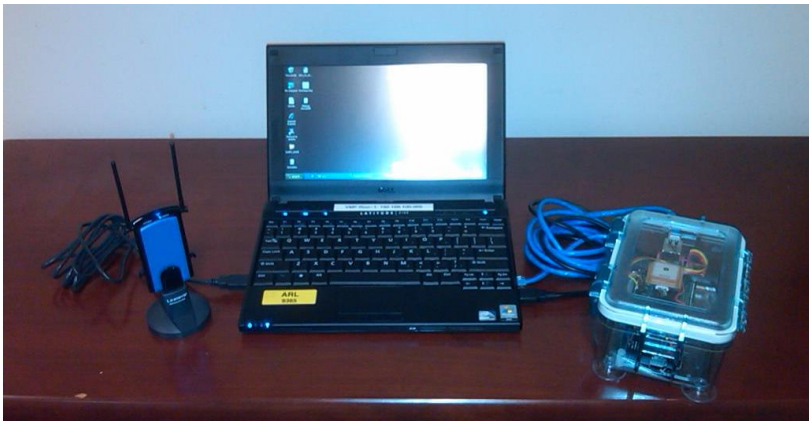

Figure 4.5. The components of the prototype GPS-based collision detection system used in field testing

Three full prototype boxes were assembled to perform tests with three vehicles operating in convoy formation. Each vehicle's computer is able to receive information from the other two vehicles simultaneously, so each vehicle can perform its own collision detection and warning.

4.5 Comments on the Proposed System

With this GPS-V2V approach, the driving environment detection specifications outlined in Table 2.1 remain quite useful. Notice that "range accuracy" requires measurements with less than 1 m error. The absolute positioning accuracy of low-cost GPS receivers is not on the order of 1 meter but rather between 3 and 10 meters. However, it was described earlier that the worst error sources are spatially and temporally correlated for GPS receivers that are not far apart [**20**]. Thus, the relative positioning measurements between two receivers can be calculated accurately despite poor absolute positioning accuracy [**24**]. Since a collision warning system relies on relative measurements alone, the correlation between GPS receivers is convenient for this application. Research is ongoing to quantify the accuracy of the headway distance calculated from the GPS receivers. For these tests, the measured headway distance will be compared to the range measurement from a Sick LIDAR that is mounted to one of the vehicles. This research is also listed in the Future Work section of this thesis.

Chapter 5

Initial Field Testing and Data Collection

This chapter documents the field testing phase of the project, including data collection and preliminary assessment of the feasibility of the proposed system concept. The first tests were performed at and around Penn State University in State College, PA. More in-depth field tests were performed at Yuma Proving Grounds in Yuma, AZ to evaluate the initial performance of the proposed system in actual military convoy situations.

5.1 Testing at Penn State University

The prototype sensor boxes were installed on three passenger vehicles for testing at Penn State University. The first tests consisted of driving the vehicles on nearby roads and highways in State College, PA to check the basic operation of the system: ensure network connectivity, data transmission, sanity of the warning indicator, etc. The GPS trace from one of these tests is shown in Figure 5.1. For all of the following tests, the GPS position and forward velocity were recorded by the prototype system on each vehicle, along with the longitudinal, lateral, and vertical accelerations measured by the MEMS accelerometer.

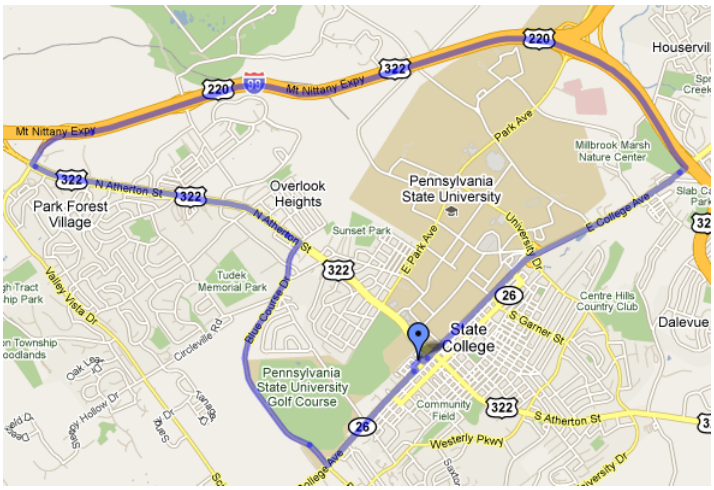

Figure 5.1. Google Maps view of a GPS trace from a convoy test performed around State College, PA

Three-vehicle convoy tests were also performed at the Thomas D. Larson Pennsylvania Transportation Institute (LTI) test track. The test track provided a closed circuit on which to drive in convoy formation and perform sudden braking maneuvers. An aerial view of the track is presented in Figure 5.2.

Figure 5.2. An aerial view of the Thomas D. Larson Pennsylvania Transportation Institute test track

For the tests at LTI, the drivers were instructed to drive between 30 and 40 mph in a convoy formation where all vehicles traverse the same path in a single column. During each lap, upon entering a straight section of the test track, the leader was instructed to brake to a complete stop at

varying levels of deceleration. The followers were instructed to spread into different lanes in the braking zone (for safety reasons) and respond to the leader's braking with natural driving behavior. The collision warning indicator was operating during all testing but was invisible to the drivers, thus the results represent a blind test to the participants.

The purpose of these tests at LTI was to assess the adequacy of the warning parameter in preventing a possible rear-end collision. By comparing the braking actions of the drivers to the warnings issued by the prototype system, it can be seen whether the proposed GPS-based collision warning system is feasible. The time delay is measured between the braking actions of the two vehicles and compared to the timeliness of the warning issued by the prototype system. In this case, the feasibility threshold is determined by ensuring that the warning from the system always precedes the driver reaction. More extensive testing and discussion on the timeliness of warnings is given in later chapters.

As a reminder, the safe/danger decision algorithm used in all the tests is outlined in Equation (8.2). Table 5.1 presents the values of all tunable parameters included in the algorithm. The following figures display data from one of the tests at LTI. Figure 5.3 gives a GPS outline of the test track, as collected by the three vehicles involved in the test. Figure 5.4 shows each vehicle's velocity profile for the duration of the test. Notice that this specific test included three aggressive brakes to a complete stop. Figure 5.5 and Figure 5.6 give the headway distance and corresponding warning parameter value, respectively, as reported to the second and third vehicles. These plots are given so that the general system operation can be seen for some of the testing at LTI.

Table 5.1. Values for the tunable parameters in the collision warning algorithm that were used during field testing at LTI test track

Parameter	Value
Maximum Deceleration, α	8 m/s^2
Time Delay, τ	1.4 s
Distance Buffer, d_0	5 m
Friction Coefficient, μ	0.8
Minimum Friction, $\mu_{\min}$	0.2
Friction Norm, μ_{norm}	1
Minimum Factor, $f(\mu_{\min})$	2

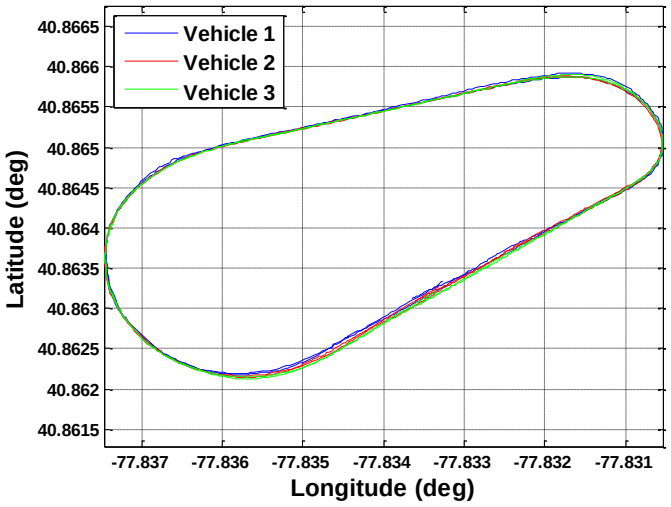

Figure 5.3. GPS outline of the LTI test track

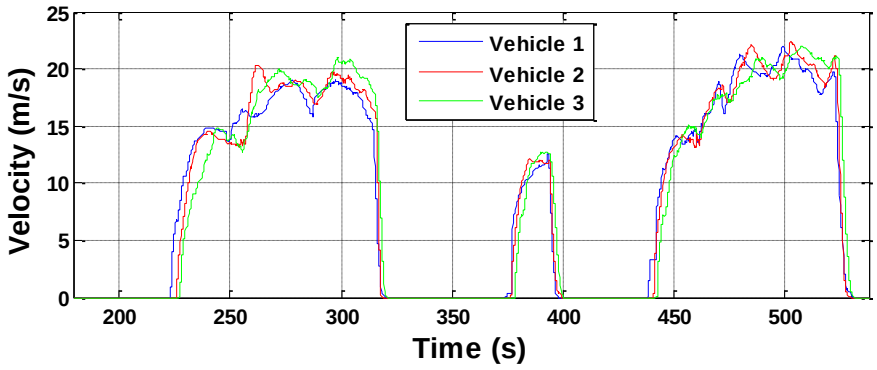

Figure 5.4. Velocity profiles for the three vehicles during testing at LTI

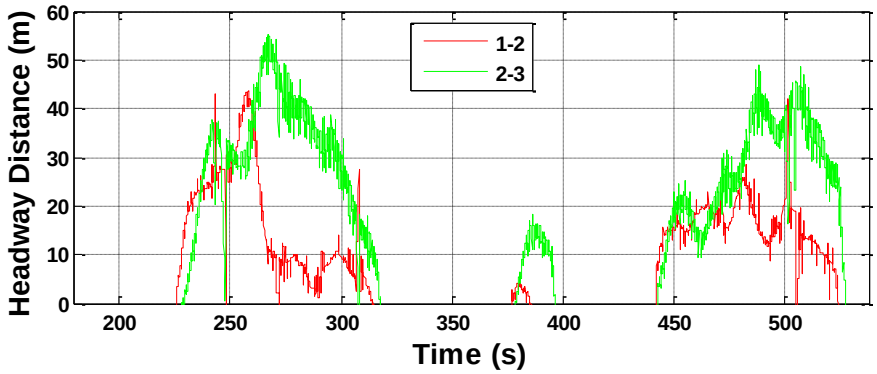

Figure 5.5. Headway distance between the vehicles during testing at LTI

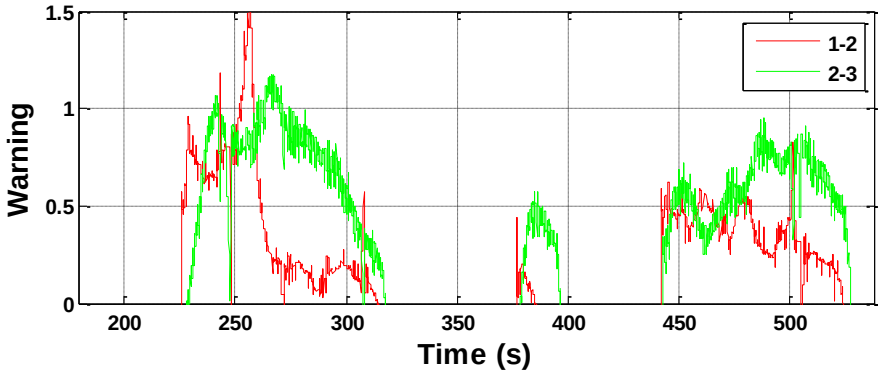

Figure 5.6. Warning parameter values for the second and third vehicles during testing at LTI

5.2 Testing at Yuma Proving Grounds

More extensive tests were performed at Yuma Proving Grounds (YPG) in Yuma, AZ. The prototype systems were installed on three Oshkosh Palletized Loading System (PLS) trucks, shown in Figure 5.7. Testing at Yuma with the PLS trucks provided an opportunity to analyze the proposed system's performance in actual military convoy environments. There is open sky visibility for the GPS receivers at all locations at YPG.

Figure 5.7. The PLS trucks used for field testing at Yuma Proving Grounds

Five different courses were used for three-vehicle convoy driving tests at Yuma. The five courses are outlined below, along with the types of tests performed on them. The speeds used for testing varied depending on the course, but it all cases the speed was representative of normal convoy driving.

Laguna Levels West Trails – This consists of winding sand/dirt course with minor elevation changes. Laps were driven in normal convoy formation, and panic stop tests were performed in single column formation.

Shipmen Street – This is a street at YPG with rough pavement and smooth pavement at opposite ends. Panic stop tests were performed in single column formation.

Laguna Hills Trail – This is a winding rocky/dirt course with significant inclines and blind crests. Laps were driven in normal convoy formation.

Course B – This is a rectangular course with paved roads on long sides and dusty roads on short sides. Laps were driven in normal convoy formation, and panic stops as well as speed-changing tests were conducted in staggered formation.

Airfield Tarmac – This is a large concrete pad used for aircraft loading. Panic stop tests were conducted in staggered formation.

Like the tests at LTI, the purpose of the tests at YPG was to assess the adequacy of the warning parameter in preventing a possible rear-end collision. However, testing at YPG also allowed for the examination of system performance in dusty conditions. Figure 5.8 shows the low visibility caused by dust along the pathway. Once again, the safe/danger decision algorithm used in all the tests is outlined in Equation (8.2). The tunable parameters used for the tests at YPG are the same as those given in Table 5.1, except the friction coefficient was often modified to reflect driving on dirt, sand, or gravel.

Figure 5.8. A view of the preceding vehicle from inside the cab of a PLS truck during testing at YPG

The following figures display data from one of the tests at YPG. Figure 5.9 gives a GPS outline of the Laguna Levels West Trails, as collected by the three vehicles involved in the test. Figure 5.10 shows each vehicle's velocity profile for the duration of the test. Figure 5.11 and Figure 5.12 give the headway distance and corresponding warning parameter value, respectively, as reported to the second and third vehicles. These plots are given so that the general system operation can be seen for some of the testing at YPG.

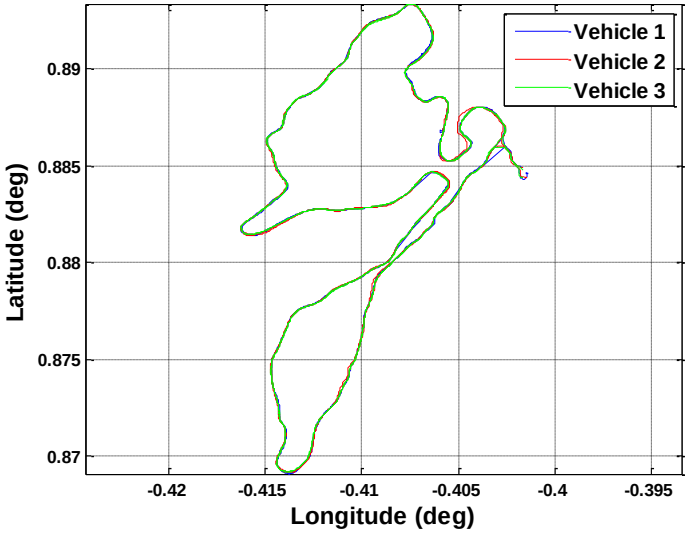

Figure 5.9. GPS outline of the Laguna Levels West Trails course

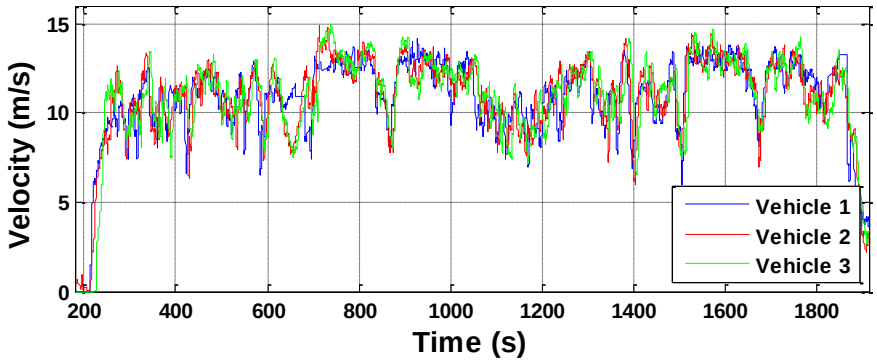

Figure 5.10. Velocity profiles for the three vehicles during testing at YPG

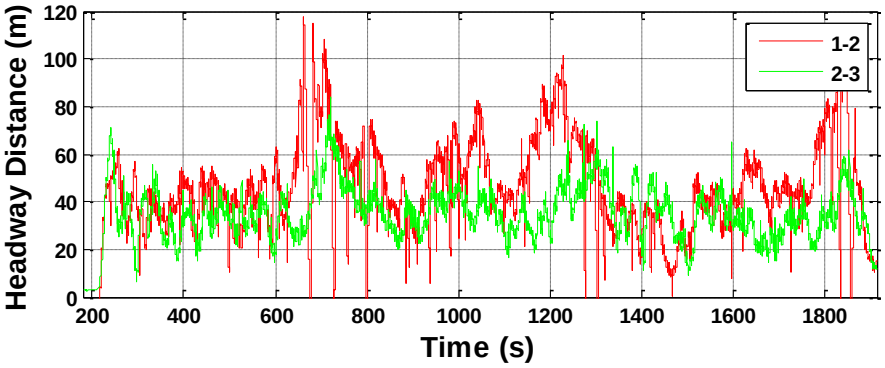

Figure 5.11. Headway distance between the vehicles during testing at YPG

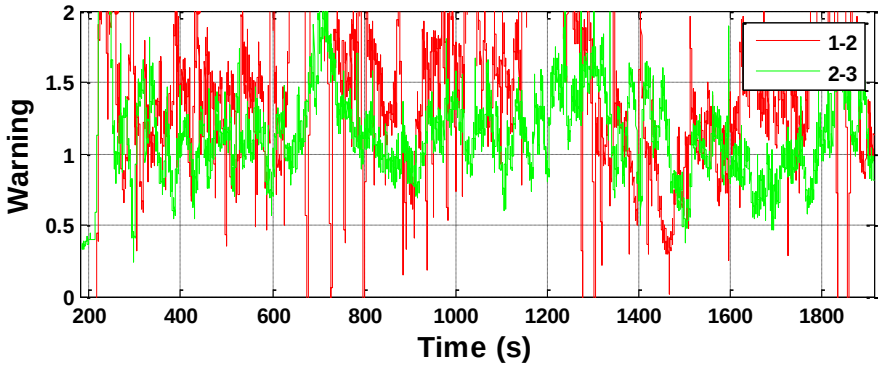

Figure 5.12. Warning parameter values for the second and third vehicles during testing at YPG

5.3 Sample Test Events

At this point, it is beneficial to examine in detail a sudden braking event within a two-vehicle convoy that led to a safe stop and a similar event that resulted in a collision. Two different test events that were performed at the LTI test track are examined below. The data presented for each test is from the GPS receivers alone. The accelerometer measurements were recorded during these tests but were not used in the collision warning algorithm.

5.3.1 A Safe Stop Event

Figure 5.13 through Figure 5.15 present a scenario where two vehicles traveling in convoy formation at 20 m/s braked to a complete stop. While the second vehicle was following closely to the first vehicle – a headway distance of 15 m and warning parameter value of 0.31 – the driver reacted within 0.4 s to the aggressive braking action by the first vehicle. The second vehicle experienced a near-constant deceleration at 4 m/s^2 and came to a complete stop safely behind the first vehicle. Despite the severe value of the warning parameter when the first vehicle started to brake (well below the safe value of 1), the second driver reacted quickly enough to brake safely. The parameters from Table 5.1 used in the collision warning algorithm are very conservative. Notice that the value for the time delay is 1.4 seconds but the second driver reacted within 0.4 seconds.

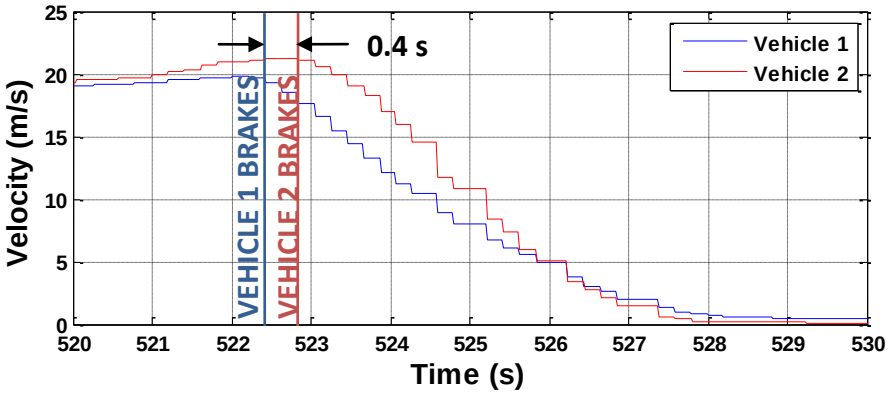

Figure 5.13. Velocities of the first and second vehicle during the safe stop event

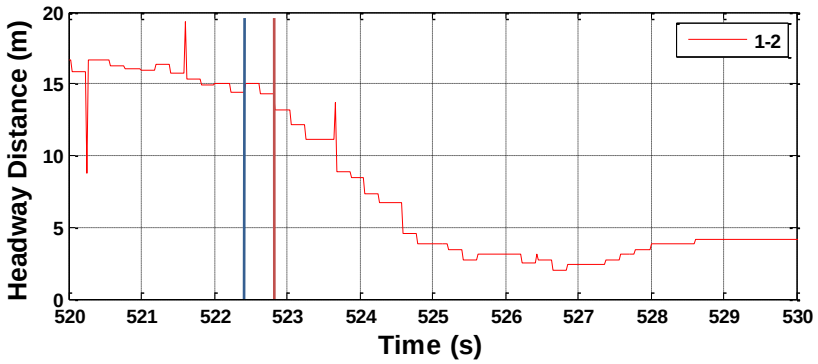

Figure 5.14. Headway distance between the first and second vehicle during the safe stop event

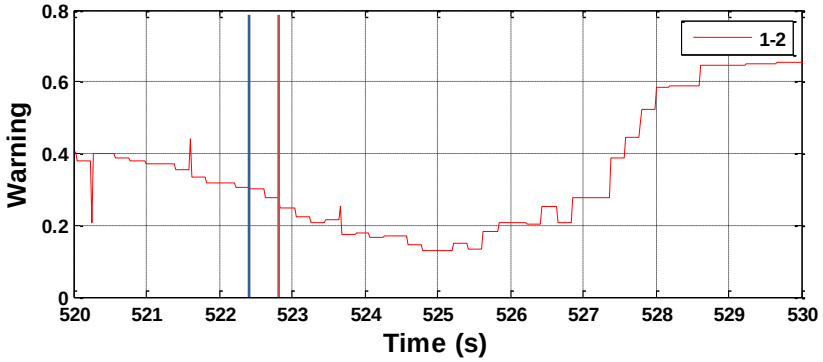

Figure 5.15. Warning parameter for the second vehicle issued by the collision detection system during the safe stop event

5.3.2 A Rear-end Collision Event

Now examine a similar situation that resulted in a rear-end collision, presented in Figure 5.16 through Figure 5.18. Both vehicles were traveling in convoy formation at 16 m/s with their current headway distance near 10 m.

Like the previous case, the second vehicle was following too closely to the first vehicle for the current speed – this can be seen by the extreme value of the warning parameter. However, unlike the previous case, the second driver took an extra second to react to the braking action of the first vehicle. This extra second was caused by driver distraction. Notice that 1.4 seconds elapsed between the initial braking action of the first vehicle and the initial braking action of the second vehicle. Also notice that the warning parameter for the second vehicle displayed a value of 0.20 at the time the first vehicle began braking, and that it increased in severity simultaneously with the braking action of the first vehicle. By the time the second driver became aware of the situation and began to brake, the warning parameter reached a value below 0.1 and the headway distance was only a few meters. At this point, collision was inevitable. The front bumper of the second vehicle came to a stop "past" the rear bumper of the first vehicle. The warning parameter predicted an unsafe situation all along – it reacted instantaneously to the braking of the first vehicle, much faster than the second driver reacted.

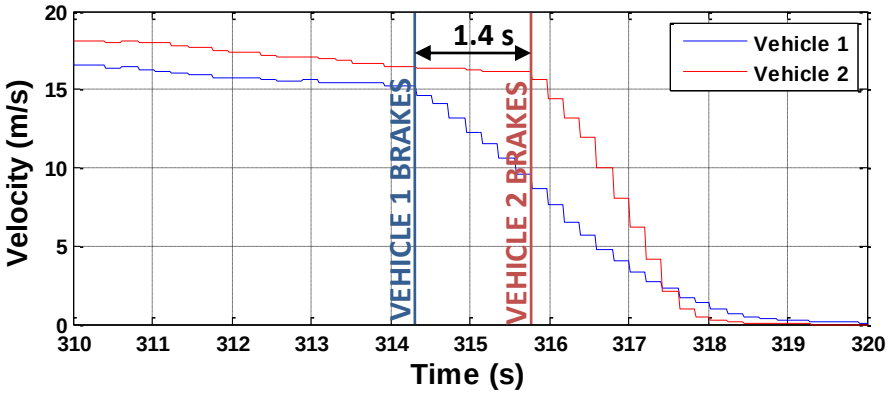

Figure 5.16. Velocities of the first and second vehicles during the collision event

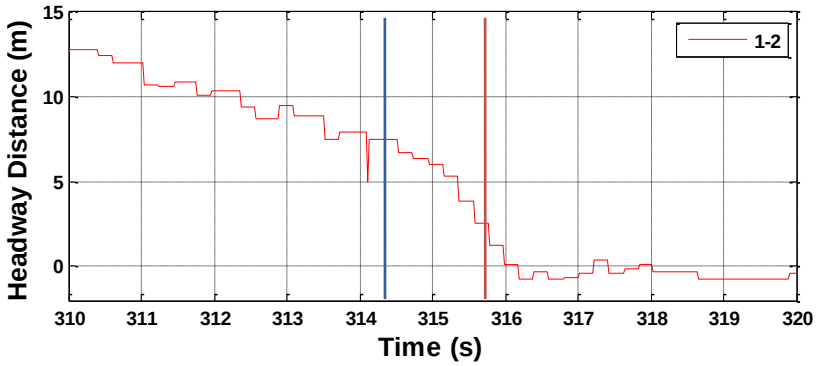

Figure 5.17. Headway distance between the first and second vehicles during the collision event

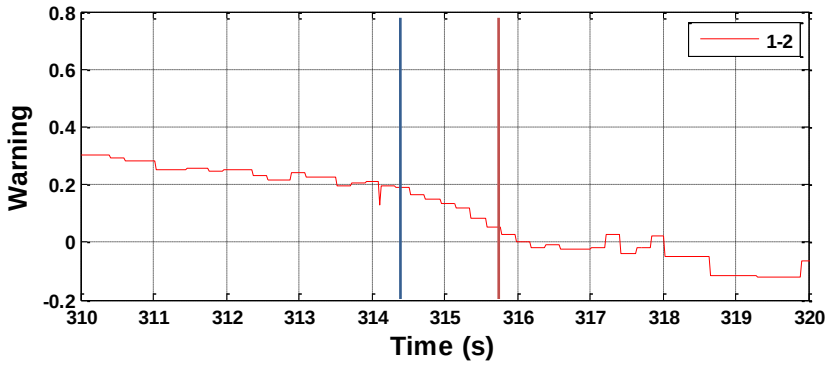

Figure 5.18. Warning parameter for the second vehicle issued by the collision detection system during the collision event

These results show the adequacy of the GPS collision detection system in predicting the impending collision. In this case, driver distraction caused the collision. However, the extra second of delay can be from many other causes including low visibility, driver fatigue, and unfamiliarity with the vehicle. If the warning parameter was available to the second driver, this collision could have been prevented.

5.4 Summary of the Initial Field Tests

The three-vehicle tests at LTI and YPG included multiple events where all vehicles aggressively braked to a complete stop in convoy formation. Figure 5.19 presents the results of these brake tests from panic stop tests performed at LTI and the YPG airfield tarmac. Each point on the plot represents the response delay between the initial braking action of the leader vehicle and the initial braking action of the follower vehicle. The corresponding warning parameter value for the instant at which the leader vehicle began braking is also given. Green circular points represent safe stop events where the follower did not breach the 5 m buffer distance between vehicles. Orange triangle points represent safe stop events where the follower breached the 5 m buffer distance but did not collide. The red stars represent collision events that were recorded.

The results of this plot stress the importance of a timely warning and support the feasibility of a GPS-based collision detection system. The extra second of driver delay that separates the collision event from the safe stop events could have been eliminated with the warning given by the prototype GPS-based system used in testing.

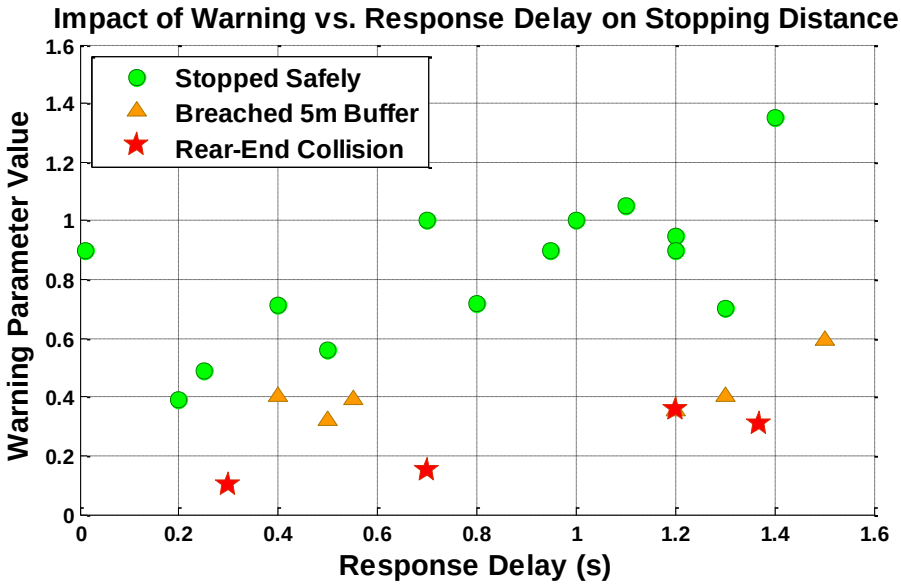

Figure 5.19. The impact of warning parameter severity and response delay on stopping distances between two vehicles in a convoy

For military convoys operating in heavy dust or other low visibility conditions, slow reaction times by follower vehicles are not uncommon. Convoy drivers cannot always rely on visual feedback to brake safely. The seconds saved by warnings from the proposed GPS-based system would be extremely valuable in these situations.

Still, there is wide-spread concern that using GPS alone is not practical for a rear-end collision detection system. In the next chapter, measurements from the accelerometer are examined in how they improve the performance of the proposed system. More specifically, the next chapter will discuss how the GPS and accelerometer measurements can be fused in a Kalman filter to improve the vehicle estimation for this application.

Chapter 6

Background on Kalman Filtering

This chapter explains the framework for a Kalman filter that will be used to improve vehicle state estimation for collision warning. The Kalman filter equations are presented, followed by a short discussion on the mechanization equations and error characteristics that are needed to implement the filter with the proposed collision warning system.

6.1 Discrete-time Kalman Filter

Kalman filters are among the most common estimators, and under certain assumptions, they provide an optimal, unbiased method for estimation. Essentially, the Kalman filter reduces the uncertainties of zero-mean white noise disturbances to predict the state of a linear system. Through extensions to the framework, the Kalman filter can be applied to a number of other systems with disturbances that may not fit the above description. A brief history of the Kalman filter can be found in [**25**].

A discrete-time Kalman filter is employed in this thesis for the proposed collision detection system. A discrete-time filter implementation is appropriate since the collision detection system operates on a fixed, scheduled time interval that is managed by the computer. The Kalman filter consists of five essential stages that repeat every time interval of the system. The stages are outlined below [**26**], [**27**].

6.1.1 State Estimate Extrapolation (Propagation)

The current state estimate (formed from the observations up to and including the current time) is used to compute the predicted value of the state at the next time interval. This is the first part of the extrapolation step, often called the propagation, prediction, or forecast step.

6.1.2 Covariance Estimate Extrapolation (Propagation)

Similar to the state estimate extrapolation, the current state covariance estimate is used to compute the predicted value of the state covariance at the next time interval. This is the second part of the extrapolation step.

6.1.3 Filter Gain Computation

Using the extrapolated state covariance estimates from the previous stage, the filter gain is computed. The filter gain is directly related to the relative accuracy of the extrapolated state versus the measurement found at the current time interval. A high filter gain means that the current measurement is regarded as "more accurate" than the extrapolated state estimate. A low gain means that the extrapolated state estimate is believed to be "more accurate" than the measurement [**26**].

6.1.4 State Estimate Update

Before the state estimate is updated, the extrapolated state estimate is used to predict the value of the current measurement. It is then subtracted from the actual value of the current measurement. This difference is called the "innovation." Then, the state estimate is updated using the innovation, filter gain, and extrapolated state estimate. This is the first part of the update step, often called the corrector or data-assimilation step.

6.1.5 Covariance Estimate Update

The state covariance estimate is updated using the extrapolated state covariance estimate. This is the second part of the update step.

6.2 Kalman Filter Equations

First consider a linear dynamic system in continuous time with a measurement equation. The disturbance input vector, **w**(*t*), and measurement error vector, **n**(*t*), are white, zero-mean Gaussian random sequences that are uncorrelated with each other. **F** is the state matrix, **G** is the input matrix, and **L** is the disturbance matrix.

$$\dot{\mathbf{x}}(t) = \mathbf{F}(t)\mathbf{x}(t) + \mathbf{G}(t)\mathbf{u}(t) + \mathbf{L}(t)\mathbf{w}(t) \tag{6.1}$$

$$\mathbf{y}(t) = \mathbf{H}(t)\mathbf{x}(t) + \mathbf{n}(t) \tag{6.2}$$

The corresponding discrete time system with time step Δt and observation vector $\mathbf{z}_k$ is given as

$$\mathbf{x}_k = \mathbf{\Phi}_{k-1}\mathbf{x}_{k-1} + \mathbf{\Gamma}_{k-1}\boldsymbol{u}_{k-1} + \mathbf{\Lambda}_{k-1}\mathbf{w}_{k-1} \tag{6.3}$$

$$\mathbf{z}_k = \mathbf{H}_k\mathbf{x}_k + \mathbf{n}_k \tag{6.4}$$

where the noise vector properties are

$$\mathbf{w}_k \sim N(0, \mathbf{Q}_k^{'}) \tag{6.5}$$

$$\mathbf{n}_k \sim N(0, \mathbf{R}_k) \tag{6.6}$$

$$E\left(\mathbf{w}_k \mathbf{n}_j^T\right) = 0 \text{ for all } j, k \tag{6.7}$$

and where the input matrix $\mathbf{\Gamma}$, the noise matrix $\mathbf{\Lambda}$, and the state transition matrix, $\mathbf{\Phi}$, can be found by the following equations.

$$\mathbf{\Phi}(\Delta t) = e^{\mathbf{F}\Delta t} \tag{6.8}$$

$$\mathbf{\Gamma}(\Delta t) = \mathbf{\Phi}(\mathbf{I}_n - \mathbf{\Phi}^{-1})\mathbf{F}^{-1}\mathbf{G} = (\mathbf{\Phi} - \mathbf{I}_n)\mathbf{F}^{-1}\mathbf{G} \tag{6.9}$$

$$\mathbf{\Lambda}(\Delta t) = \mathbf{\Phi}(\mathbf{I}_n - \mathbf{\Phi}^{-1})\mathbf{F}^{-1}\mathbf{L} = (\mathbf{\Phi} - \mathbf{I}_n)\mathbf{F}^{-1}\mathbf{L} \tag{6.10}$$

If $\mathbf{F}$ is singular, then the following approximations can be used in place of Equations (6.9) and (6.10).

$$\mathbf{\Gamma}(\Delta t) = \mathbf{\Phi}\left[\mathbf{I}_n - \left(\frac{1}{2}\right)\mathbf{F}\Delta t + \left(\frac{1}{3!}\right)\mathbf{F}^2\Delta t^2 - \cdots\right]\mathbf{G}\Delta t \tag{6.11}$$

$$\mathbf{\Lambda}(\Delta t) = \mathbf{\Phi}\left[\mathbf{I}_n - \left(\frac{1}{2}\right)\mathbf{F}\Delta t + \left(\frac{1}{3!}\right)\mathbf{F}^2\Delta t^2 - \cdots\right]\mathbf{L}\Delta t \tag{6.12}$$

Before the Kalman filter equations can be applied, the initial conditions of the system must be known. The expected values of the initial state and its covariance are denoted by

$$E(\mathbf{x}_0) = \hat{\mathbf{x}}_0 \tag{6.13}$$

$$E[(\mathbf{x}_0 - \hat{\mathbf{x}}_0)(\mathbf{x}_0 - \hat{\mathbf{x}}_0)^T] = \mathbf{P}_0 \tag{6.14}$$

Now the Kalman filter equations can be applied. Equation (6.15) shows the state estimate extrapolation, denoted by (−). The (−) and (+) symbols denote the pre and post-update estimates of a state.

$$\hat{\mathbf{x}}_k(-) = \mathbf{\Phi}_{k-1}\hat{\mathbf{x}}_{k-1}(+) + \mathbf{\Gamma}_{k-1}\mathbf{u}_{k-1} \tag{6.15}$$

The covariance estimate extrapolation is given by

$$\mathbf{P}_k(-) = \boldsymbol{\Phi}_{k-1}\mathbf{P}_{k-1}(+)\boldsymbol{\Phi}_{k-1}^T + \mathbf{Q}_{k-1} \tag{6.16}$$

$$\text{where } \mathbf{Q}_k = \boldsymbol{\Lambda}_k \mathbf{Q}_k^{'} \boldsymbol{\Lambda}_k^T \tag{6.17}$$

The filter gain computation follows, as shown below.

$$\mathbf{K}_k = \mathbf{P}_k(-)\mathbf{H}_k^T\left[\mathbf{H}_k\mathbf{P}_k(-)\mathbf{H}_k^T + \mathbf{R}_k\right]^{-1} \tag{6.18}$$

Now the update step can be executed, starting with the state estimate update.

$$\hat{\mathbf{x}}_k(+) = \hat{\mathbf{x}}_k(-) + \mathbf{K}_k[\mathbf{z}_k - \mathbf{H}_k\hat{\mathbf{x}}_k(-)] \tag{6.19}$$

The covariance estimate update is the final stage of the Kalman filter cycle for time interval *k*.

$$\mathbf{P}_k(+) = \left[\mathbf{P}_k(-)^{-1} + \mathbf{H}_k^T\mathbf{R}_k^{-1}\mathbf{H}_k\right]^{-1} \tag{6.20}$$

The same steps are then executed for the time interval *k*+1, and so on.

Figure 6.1 presents a block diagram of the discrete-time Kalman filter. Notice the "delay" blocks that represent the recursive nature of the filter, moving from one time step to the next. Also notice that the filter gain computation and covariance estimator are separate from the state estimator. This separation is because the filter gain and covariance have no dependence on the input and observation vectors. The filter gain computation and covariance extrapolation and update could be performed offline, given the time variations in the system and its statistics, and stored for each time interval *k*. Then, real-time implementation of the Kalman filter would be reduced to state estimation only.

6.3 Kalman Filter Setup

There has been much previous work done on the integration of GPS and Inertial Navigation Systems (INS), especially for vehicle applications [**28**], [**29**], [**30**], [**31**]. Almost all previous research has focused on two-dimensional or three-dimensional state estimation. In the case of the proposed collision detection system, it was identified earlier that only one dimension is of interest – that along the path of travel. Hence, the states of interest for an individual vehicle are only those along the vehicle's longitudinal axis, namely the distance traveled, *s*, and the forward velocity, *v*. With a better estimate of these states, one can calculate improved estimates of headway distance, velocity, and relative velocity which can then be fed into the collision warning algorithm (from Equation (4.1)).

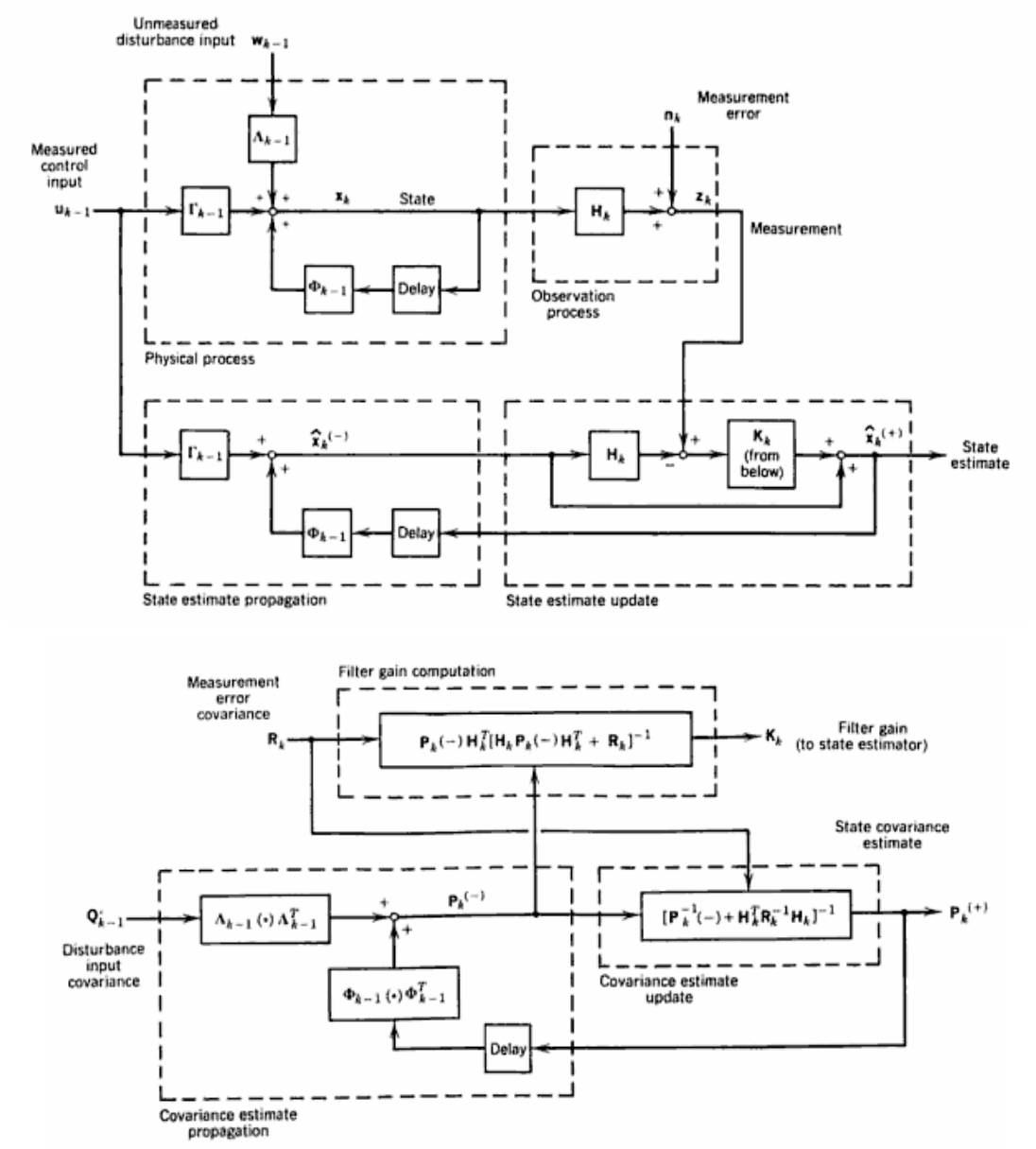

Figure 6.1. Discrete-time Kalman filter (From Stengel [27])

6.4 Characterization of Sensor Errors

The proposed low-cost collision detection system is composed of a GPS receiver and a triple-axis MEMS accelerometer. The integration of these sensors along the longitudinal axis of the vehicle is fairly simple and straightforward. Integrating the longitudinal acceleration yields the forward velocity, which, when integrated again, produces the distance traveled by the vehicle. Before the sensors can be fused in the Kalman filter, the measurement errors must be characterized for each sensor.

6.4.1 GPS Receiver

The largest source of error in GPS measurements can be attributed to the dilution of precision (DOP) that is a direct factor of the satellite constellation geometry. The position error for a GPS receiver is related to the error in measuring the pseudoranges from the GPS satellites, called user range error (URE). For the particular GPS receiver used in the prototype system, the standard deviation of the user range error (σ_{URE}) is taken to be 5 meters. A derivation of the origin of this value is given by Gupta in [**32**].

The standard deviation of the velocity measurement error from the GPS receiver (σ_v) was found to be 0.5 m/s when the velocity is constant or mildly changing [**32**]. However, the GPS update rate of 5 Hz is too slow to follow the velocity changes under aggressive accelerations and decelerations. Hence, another term should be added to the error value of the GPS receiver to include velocity errors due to the low update rate. A value of 6 m/s^2 can represent aggressive accelerations and decelerations for a vehicle. With an update interval of 0.2 seconds, this corresponds to 1.2 m/s that should be added to the error. Then, the standard deviation of the velocity error is given by

$$\sigma_v = \sigma_{static} + \sigma_{dynamic} = 0.5\,^{m}/_{s} + 1.2\,^{m}/_{s} = 1.7\,^{m}/_{s} \tag{6.21}$$

The velocity error for the GPS receiver is needed to determine the variance of the velocity measurement used in the observation equation of the Kalman filter.

6.4.2 MEMS Accelerometer

The MEMS accelerometer used in the prototype system is an inexpensive sensor, so it is prone to many sources of error including noise, bias, scale factor error, and misalignment error. The error from the MEMS accelerometer can be characterized using the Allan variance method [**33**]. This method will give values for the quantization noise, random walk, and bias instability of the accelerometer by fitting a curve to the resulting plot. This procedure is described in detail for similar accelerometers in [**32**]. The most significant error sources for a MEMS accelerometer were found to be the low frequency bias and wide-band noise.

The acceleration measurement given by the accelerometer, a, is a function of the true acceleration, a_{true}, and is written as

$$a = (1 + S_a)a_{true} + b_a + n_a \tag{6.22}$$

The low frequency bias, b_a, can be modeled by the following differential equation [**34**]

$$\dot{b}_a = -\frac{1}{T_b} b_a + n_b \tag{6.23}$$

where T_b is a correlation time constant and n_b is white noise. The scale factor can be modeled by a similar equation.

$$\dot{S}_a = -\frac{1}{T_S} S_a + n_S \tag{6.24}$$

To find the true value of acceleration, the following equation is used, derived from Equation (6.22).

$$a_{true} = \frac{(a - b_a)}{(1 + S_a)} \tag{6.25}$$

The values for the accelerometer errors were chosen to be representative of the values found previously in [**32**]. The standard deviation of the accelerometer noise (σ_a) is 0.5 m/s^2, the standard deviation of the accelerometer bias (σ_b) is 0.01 m/s^2, and the correlation time T_b is 1300 seconds.

With the sensor errors characterized, the Kalman filter equations can be applied. The following chapter presents the implementation of the Kalman filter for the proposed collision warning system.

Chapter 7

Kalman Filter Implementation and Evaluation

The previous chapter presented the equations of the Kalman filter that will be used for the proposed collision detection system. This chapter will present data collection, the implementation of the Kalman filter, and how it was refined as the results were analyzed. The main purpose of the Kalman filter for the proposed system is to provide an accurate velocity estimate for the host vehicle to be used in the collision warning algorithm.

More field testing was performed to record data that could be used to apply the Kalman filter and evaluate its performance. Previous field testing data cannot be used to evaluate the Kalman filter performance because there is no reliable measurement to be used as "truth" data for those tests.

7.1 Data Collection for Kalman Filtering Tests

Experiments were conducted at the LTI test track to collect data for evaluation of the Kalman filter. The proposed system's Kalman filter is used to estimate the states for a single vehicle so only one vehicle was used during these tests. This vehicle was a full-size pickup truck that is capable of autonomous driving; it is equipped with a steering motor, throttle and brake actuators, and a range of other sensors that are used for various vehicle dynamics studies. See Figure 7.1 for a view of the truck.

Figure 7.1. View of the truck with autonomous driving capability used for the Kalman filtering data collection

The truck is outfitted with a Novatel SPAN GPS/INS system, consisting of a Novatel DL-4 Plus GPS receiver and a Honeywell HG1700-AG17 inertial measurement unit, shown in Figure 7.2. When operating in DGPS mode with a nearby base station, this tactical-grade GPS/INS system reports position measurements within an error of 2 cm. This is the mode of operation that was used during the Kalman filter tests. For all the test runs, the data from this Novatel SPAN system is considered ground truth. The prototype collision detection system was mounted to the roof of the truck to collect GPS and accelerometer data for integration in the Kalman filter.

Figure 7.2. The components of the Novatel SPAN system: GPS antenna, DL-4 Plus receiver, and Honeywell IMU

Three different types of tests were performed at LTI to collect data for the Kalman filter evaluation. First, for Test 1, the truck was driven at a constant speed for at least one lap of the track (approximately one mile). Second (Test 2), the truck was driven for another lap at varying speeds, accomplished by frequently accelerating, braking, and coasting. The driver was instructed to perform an aggressive acceleration to 25 mph and then slam the brakes to a complete stop for Test 3. This test was repeated for the entire length of a straight section on the track. With three different types of tests, the Kalman filter can be evaluated for a range of driving situations.

The raw data that was collected during these tests is presented below. Figure 7.3 shows an outline of the LTI test track as reported by the Novatel and low-cost GPS receivers. Figure 7.4 displays the velocity profile for the truck during the three different types of test runs. The constant speed lap of the track is presented from a time of 0 to 110 seconds (Test 1). The second lap of the track at varying speeds extends to a time of 195 seconds (Test 2). The third time segment of 195 to 240 seconds shows the aggressive acceleration and deceleration tests (Test 3). Figure 7.5 shows the corresponding longitudinal acceleration profile of the truck during the same tests.

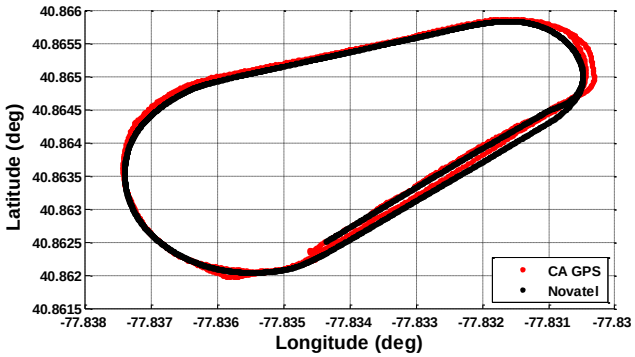

Figure 7.3. GPS outline of the LTI test track

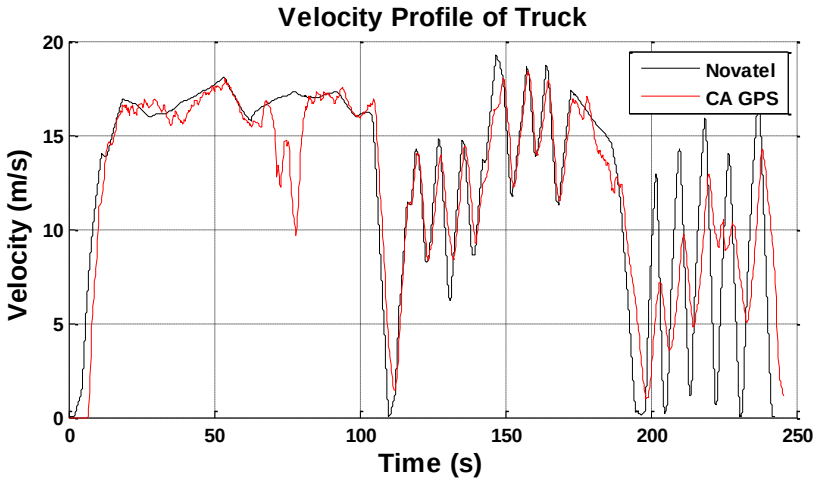

Figure 7.4. Velocity profile of the truck during the Kalman filter tests

From the velocity profile displayed above, notice the large error in the measured velocity from the low-cost GPS between the time of 70 and 80 seconds. This error is a result of the GPS losing a lock on the satellites and the dilution of precision becoming very large. Normally, this error would not occur with a clear view of the sky and the satellite constellation. In this particular area of the test track however, overhanging trees and structures block the GPS signals and may cause multipath, so the GPS measurement fidelity is decreased.

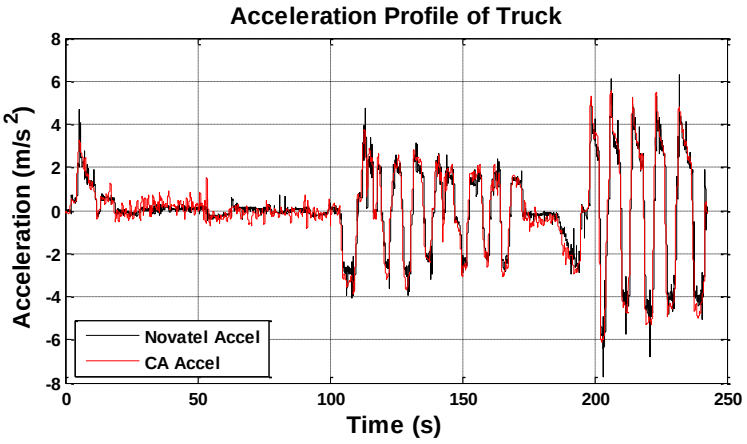

Figure 7.5. Acceleration profile of the truck during the Kalman filter tests

A view of the acceleration profile from the time 210 to 230 seconds is given in Figure 7.6. Notice that the acceleration reported by the Novatel SPAN system (derived from the DGPS velocity, not the IMU) lags the acceleration collected by the MEMS accelerometer in the prototype collision detection system. The exact source of this time lag is unknown, but is most likely due to an incorrectly-sized buffer that causes a delay in the transmission of data from the Novatel to the computer.

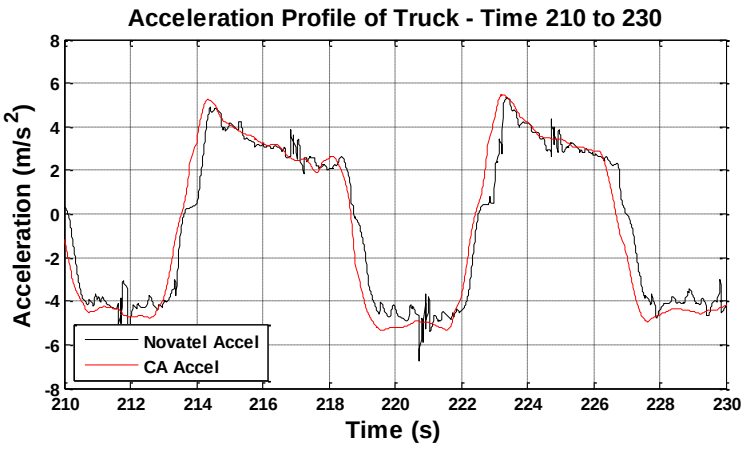

Figure 7.6. Acceleration profile of the truck between the time of 210 and 230 seconds

Regardless of the source, this lag can be accounted for by examining the cross-correlation of the two acceleration signals. The cross-correlation of two signals, x_n and y_n, can be found by:

$$R_{xy}(m) = E\{x_{n+m}y_n^*\} = E\{x_n y_{n-m}^*\} \tag{7.1}$$

The normalized cross-correlation of the two acceleration signals is presented in Figure 7.7. The acceleration derived from the Novatel lags the MEMS accelerometer by 9 indices, equivalent to 0.18 seconds. So, 0.18 seconds was added to the Novatel data to align the signals in time. The aligned acceleration measurements are given in Figure 7.8.

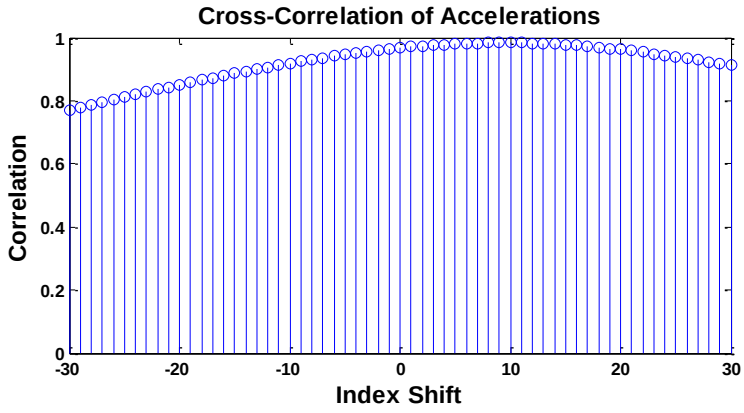

Figure 7.7. Cross-correlation of acceleration signals during the Kalman filter tests

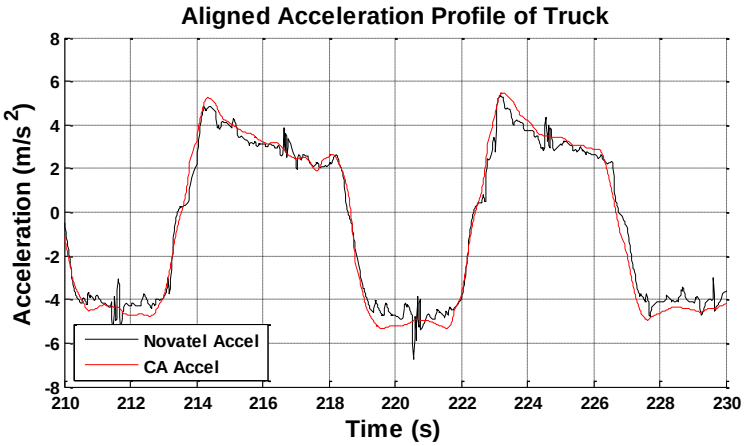

Figure 7.8. Aligned acceleration profile of the truck between the time of 210 to 230 seconds

The aligned data will be used from this point forward for all Kalman filtering analysis and evaluation. The following sections focus on comparing the performance of the Kalman filter to the raw data collected by the low-cost GPS receiver from the prototype system and to the truth data collected by the Novatel SPAN system.

7.2 Performance of the GPS Receiver Alone

Before the Kalman filter is applied to the proposed collision detection system, the raw performance of the system is examined. The velocity profile for Tests 1-3 was shown in Figure 7.4. The error in the low-cost GPS velocity measurement for these tests is now given in Figure 7.9.

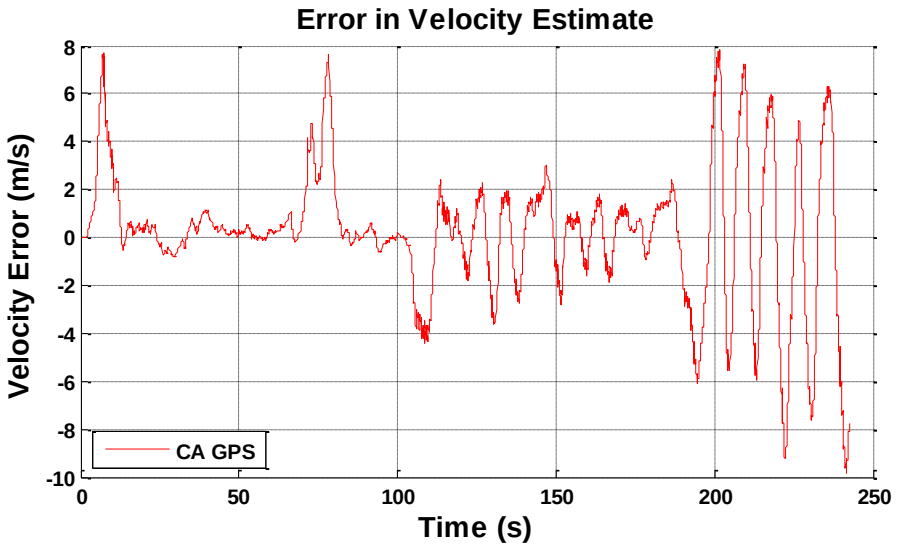

Figure 7.9. Error in the velocity measurement of the low-cost GPS

The root mean square (RMS) of the error in velocity for the low-cost GPS receiver was calculated as a measure of its accuracy in reporting velocity. As a reference, the formula for calculating the RMS is given below in Equation (7.2).

$$x_{RMS} = \sqrt{\frac{x_1^2 + x_2^2 + \cdots + x_n^2}{n}} \tag{7.2}$$

The RMS error in the low-cost GPS velocity for the entire duration of Tests 1-3 is 2.76 m/s. This value is representative of the overall accuracy of the low-cost GPS in its velocity measurement, but does not provide a good metric for determining how the receiver performed in each individual test. Thus, the velocity profiles and their corresponding errors for Tests 1-3 are shown in Figure 7.10 through Figure 7.15. The RMS error for each of these tests is reported in Table 7.1.

Table 7.1. RMS velocity errors for the low-cost GPS

	Overall	**Test 1**	**Test 2**	**Test 3**
RMS Velocity Error (m/s)	2.76	1.9753	1.6369	4.9919

The velocity error for the raw GPS receiver (disregarding the error due to the loss of GPS lock) increases as the vehicle behavior becomes more dynamic. The GPS receiver velocity is relatively accurate when the velocity is constant or mildly changing, but is very inaccurate under high accelerations and quickly-varying speeds.

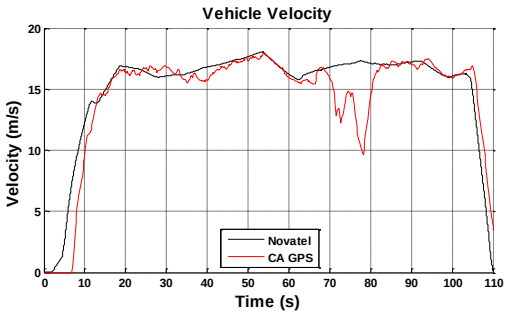

Figure 7.10. Velocity measurement of the low-cost GPS for Test 1

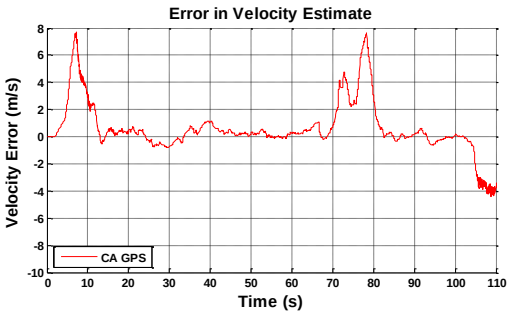

Figure 7.13. Error in the velocity measurement of the low-cost GPS for Test 1

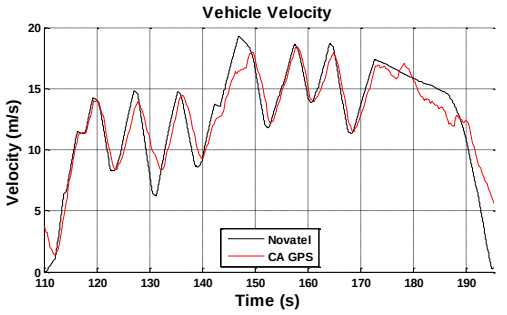

Figure 7.11. Velocity measurement of the low-cost GPS for Test 2

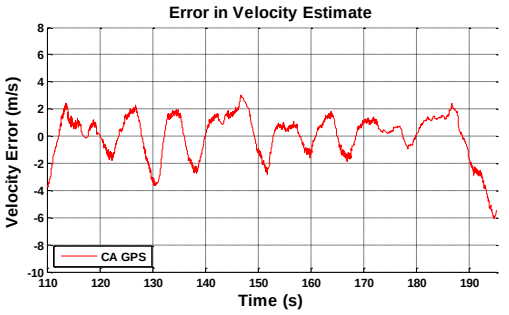

Figure 7.14. Error in the velocity measurement of the low-cost GPS for Test 2

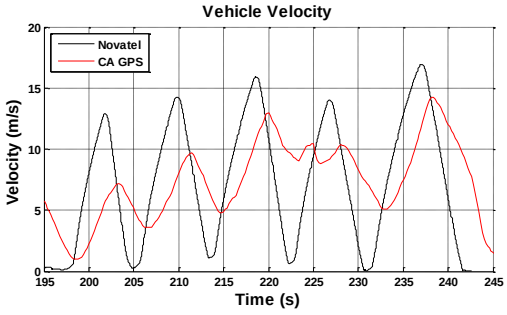

Figure 7.12. Velocity measurement of the low-cost GPS for Test 3

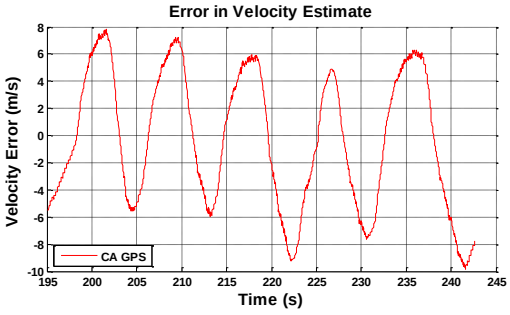

Figure 7.15. Error in the velocity measurement of the low-cost GPS for Test 3

7.3 Kalman Filter Implementation

Now that the performance of the raw data has been quantified for the proposed collision detection system, the implementation of the Kalman filter is presented. For this work, the Kalman filter was applied and evaluated offline, so that additional refinements could be made, if necessary. Presented below are the three different Kalman filter iterations that were applied to the proposed collision detection system.

The parameters used in the following Kalman filters are outlined in Table 7.2. Some parameters were adapted from values found by Gupta in [**32**].

Table 7.2. Parameters used in the Kalman filters

Parameter	**Value**
Time Interval (Δt)	0.02 s
Velocity Std Dev – Static ($\sigma_{v,static}$)	0.5 m/s
Velocity Std Dev – Dynamic ($\sigma_{v,dynamic}$)	1.2 m/s
Velocity Std Dev (σ_v)	1.7 m/s
Acceleration Std Dev (σ_a)	0.5 m/s^2
Acceleration Bias Std Dev (σ_b)	0.01 m/s^2
Bias Correlation Time (T_b)	1300 s
Dilution of Precision (DOP)	2

7.3.1 Kalman Filter #1

The first implementation of the Kalman filter on the proposed collision detection system is the simplest filter for fusing the vehicle's velocity and acceleration. The state vector for the Kalman filter becomes

$$\mathbf{x} = \begin{bmatrix} s \\ v \end{bmatrix} \tag{7.3}$$

The longitudinal acceleration *a*, measured by the MEMS accelerometer, is used as an input to the system. The linear dynamic system is written as

$$\frac{d}{dt}\begin{bmatrix} s \\ v \end{bmatrix} = \begin{bmatrix} 0 & 1 \\ 0 & 0 \end{bmatrix}\begin{bmatrix} s \\ v \end{bmatrix} + \begin{bmatrix} 0 \\ 1 \end{bmatrix} a + \begin{bmatrix} 0 \\ 1 \end{bmatrix} w \tag{7.4}$$

Since GPS forward velocity is easily obtained, it becomes the lone element in the observation, *z*. The Kalman filter equations (Equations (6.15) – (6.20)) can now be executed for this system.

$$z = \begin{bmatrix} 0 & 1 \end{bmatrix}\begin{bmatrix} s \\ v \end{bmatrix} + n \tag{7.5}$$

For this Kalman filter, the noise characteristics are outlined below. The value for DOP is multiplied by the velocity error variance because the error in the velocity measurement is directly related to the satellite constellation geometry [**32**]. A less desirable geometry will yield a less accurate measurement.

$$Q_k' = \sigma_a^2 \tag{7.6}$$

$$R_k = \sigma_v^2 * DOP \tag{7.7}$$

The velocity estimate from the Kalman filter is presented in Figure 7.16 along with the truth velocity collected by the Novatel SPAN system. This figure captures Tests 1 through 3, the same tests that were described in the previous chapter. Figure 7.17 shows the error in the velocity estimate for the duration of these tests. Figure 7.18 through Figure 7.20 show the velocity estimate from each of the tests individually. The corresponding figures, Figure 7.21 through Figure 7.23, present the error in the velocity estimate for each of the separate Tests 1 – 3. Table 7.3 shows the RMS error values for the velocity estimate.

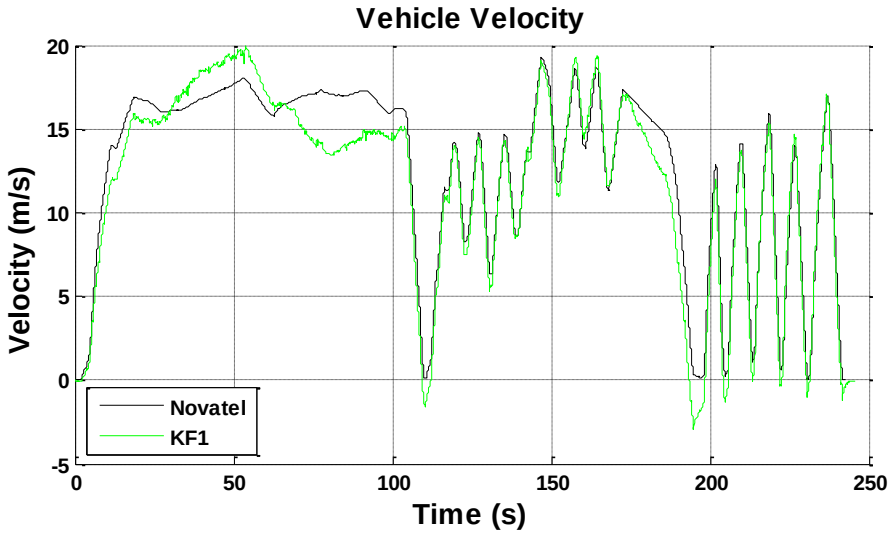

Figure 7.16. Velocity estimate from Kalman Filter #1

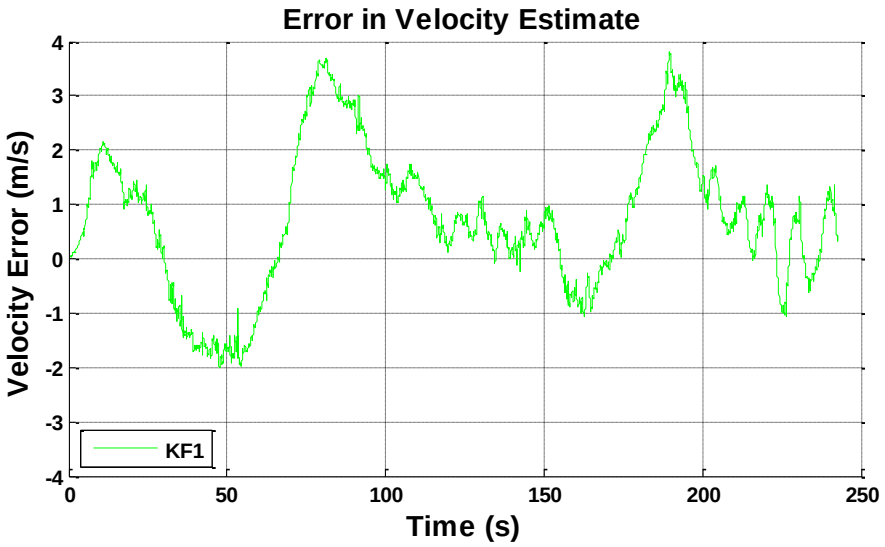

Figure 7.17. Error in the velocity estimate from Kalman Filter #1

Table 7.3. RMS velocity errors for Kalman Filter #1

	Overall	**Test 1**	**Test 2**	**Test 3**
RMS Velocity Error (m/s)	1.5031	1.7872	1.3161	1.0179

It can be seen from Figure 7.17 that the velocity error between the times of 100 to 150 seconds and 200 seconds to 245 seconds (time segments defined by repetitive acceleration and deceleration) has a steady offset. This offset is caused by the accelerometer bias that was mentioned as a significant source of error in the previous chapter. By estimating this bias term in the Kalman filter, the velocity error should be reduced. Kalman Filter #2 that follows incorporates a bias estimate.

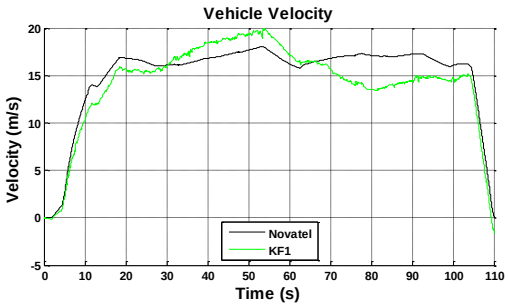

Figure 7.18. Velocity estimate from Kalman Filter #1 for Test 1

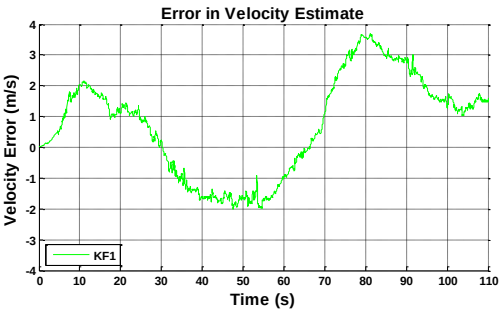

Figure 7.21. Error in velocity estimate from Kalman Filter #1 for Test 1

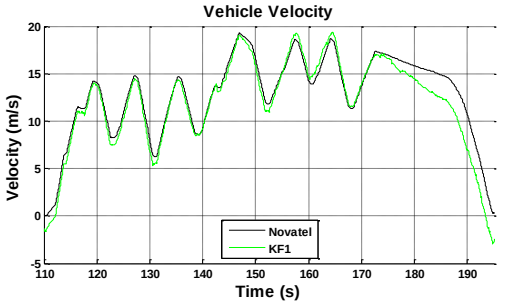

Figure 7.19. Velocity estimate from Kalman Filter #1 for Test 2

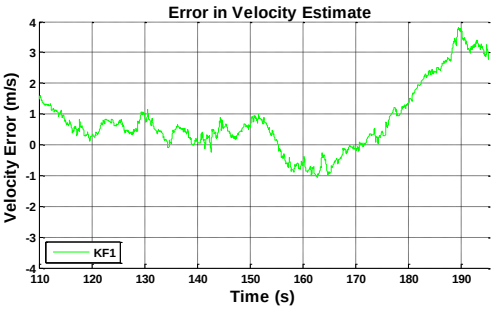

Figure 7.22. Error in velocity estimate from Kalman Filter #1 for Test 2

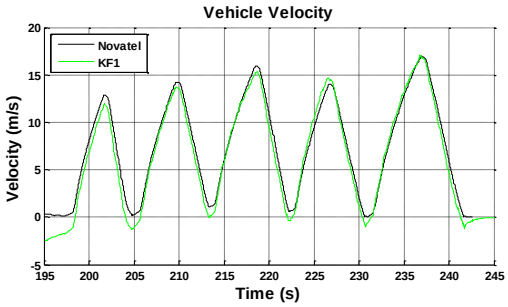

Figure 7.20. Velocity estimate from Kalman Filter #1 for Test 3

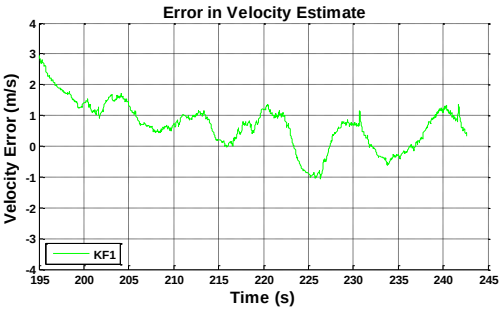

Figure 7.23. Error in velocity estimate from Kalman Filter #1 for Test 3

7.3.2 Kalman Filter #2

It was identified in the previous chapter that the accelerometer measurement can be more accurately modeled using Equation (6.25). So, the Kalman filter can be modified by updating the acceleration equation and augmenting the state vector to estimate the accelerometer bias. The scale factor is assumed to be constant (equal to zero), as it changes extremely slowly in time. The state vector for Kalman Filter #2 becomes

$$\mathbf{x} = \begin{bmatrix} s \\ v \\ b_a \end{bmatrix} \tag{7.8}$$

and the linear dynamic equation is updated and given by

$$\frac{d}{dt}\begin{bmatrix} s \\ v \\ b_a \end{bmatrix} = \begin{bmatrix} 0 & 1 & 0 \\ 0 & 0 & -\dfrac{1}{(1+S_a)} \\ 0 & 0 & -\dfrac{1}{T_b} \end{bmatrix}\begin{bmatrix} s \\ v \\ b_a \end{bmatrix} + \begin{bmatrix} 0 \\ \dfrac{1}{(1+S_a)} \\ 0 \end{bmatrix} a + \begin{bmatrix} 0 & 0 & 0 \\ 0 & 1 & 0 \\ 0 & 0 & 1 \end{bmatrix} w \tag{7.9}$$

The observation vector is similar to that given in Kalman Filter #1.

$$z = \begin{bmatrix} 0 & 1 & 0 \end{bmatrix}\begin{bmatrix} s \\ v \\ b_a \end{bmatrix} + n \tag{7.10}$$

The noise matrices for this Kalman filter are given by

$$\mathbf{Q}_k^{'} = \begin{bmatrix} 0 & 0 & 0 \\ 0 & \sigma_a^2 & 0 \\ 0 & 0 & \sigma_b^2 \end{bmatrix} \tag{7.11}$$

$$R_k = \sigma_v^2 * DOP \tag{7.12}$$

The results of Kalman Filter #2 are now presented in the same manner as Kalman Filter #1. Figure 7.24 through Figure 7.31 show the velocity estimate from the filter and its corresponding error for the entire length of the test, and for each test (Tests 1-3) individually. The RMS error values are given in Table 7.4.

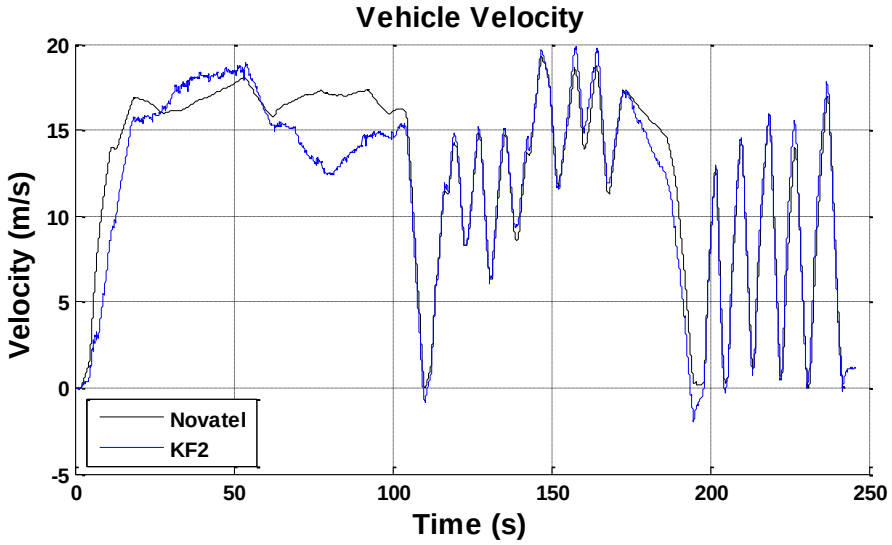

Figure 7.24. Velocity estimate from Kalman Filter #2

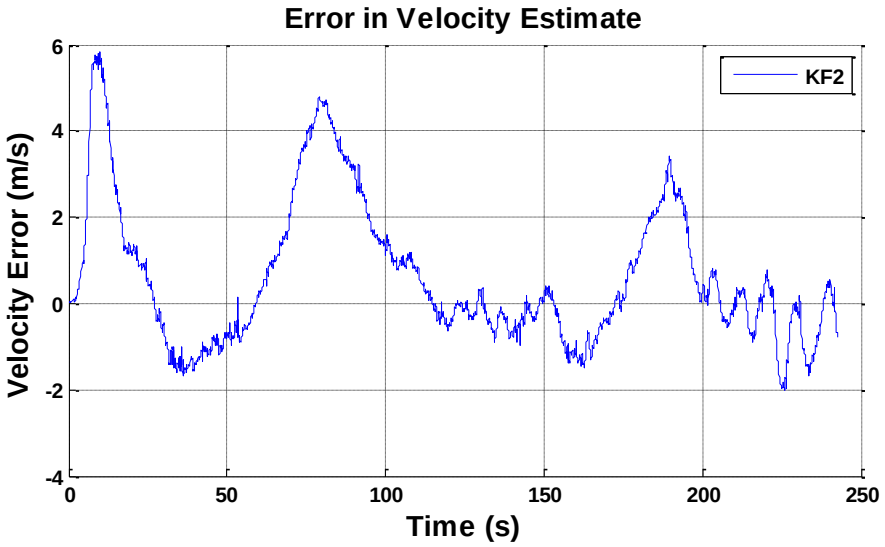

Figure 7.25. Error in velocity estimate from Kalman Filter #2

Table 7.4. RMS velocity errors for Kalman Filter #2

	Overall	**Test 1**	**Test 2**	**Test 3**
RMS Velocity Error (m/s)	1.7608	2.3678	1.1209	0.7737

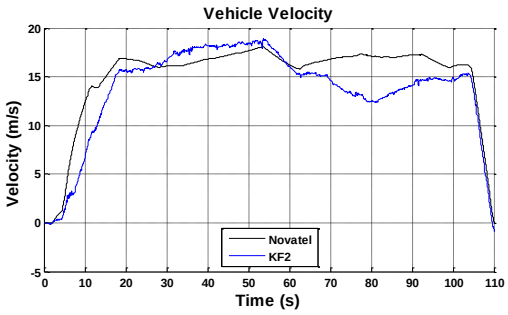

Figure 7.26. Velocity estimate from Kalman Filter #2 for Test 1

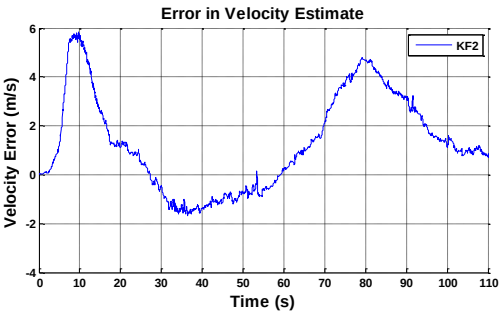

Figure 7.29. Error in velocity estimate from Kalman Filter #2 for Test 1

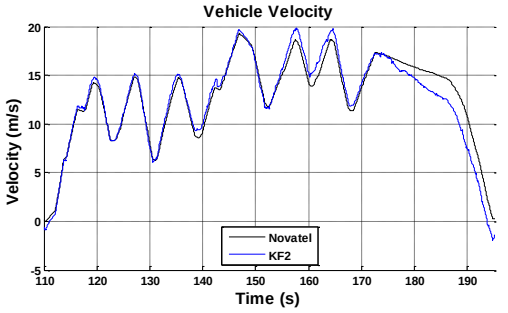

Figure 7.27. Velocity estimate from Kalman Filter #2 for Test 2

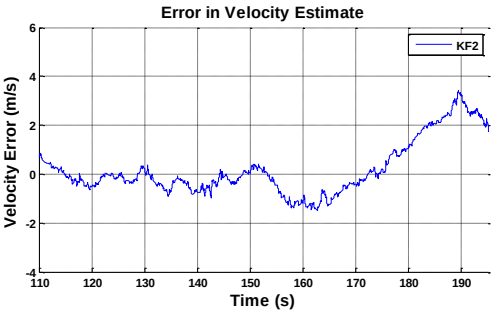

Figure 7.30. Error in velocity estimate from Kalman Filter #2 for Test 2

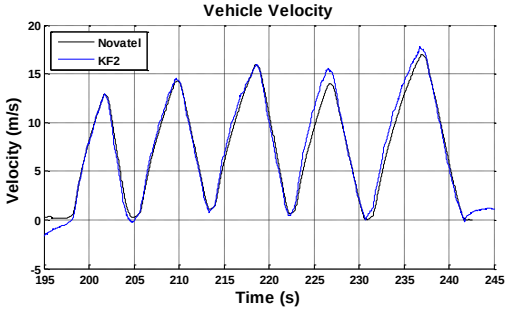

Figure 7.28. Velocity estimate from Kalman Filter #2 for Test 3

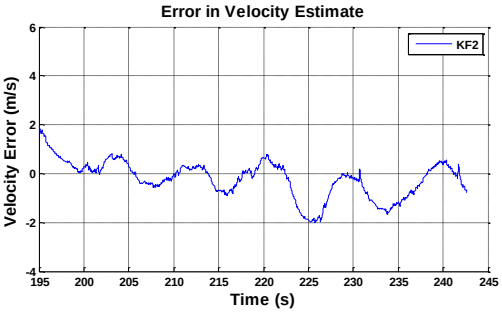

Figure 7.31. Error in velocity estimate from Kalman Filter #2 for Test 3

The accelerometer bias that was estimated by this filter is presented in Figure 7.32. The bias begins to converge around a time of 30 seconds but never reaches a steady value. This behavior is most likely due to the pitch of the vehicle and the varying road grade around the test track. Hence, the accelerometer bias acts as a crude pitch estimator and filters out some of the error in the acceleration due to the pitch.

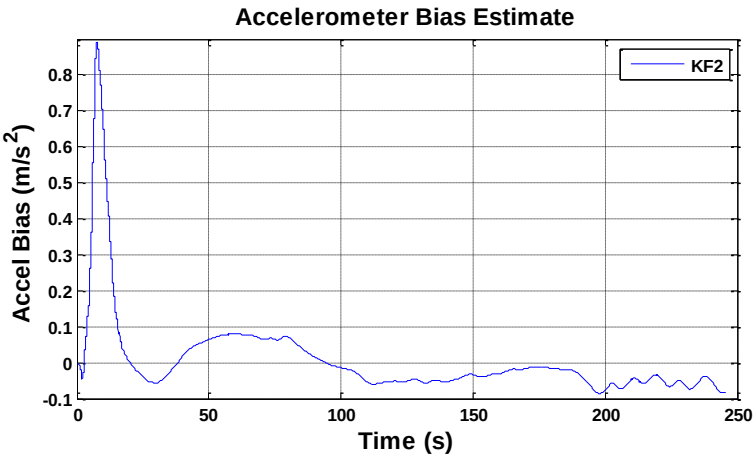

Figure 7.32. Accelerometer bias estimate from Kalman Filter #2

Notice from Table 7.4 that estimating the accelerometer bias improves the accuracy of the velocity measurement in Tests 2 and 3. However, the error for Test 1 increases from Kalman Filter #1 to Kalman Filter #2. It is even larger than the error from the raw GPS velocity measurement alone during this time. This means that the raw GPS velocity measurement is a more reliable measurement than the current Kalman filter estimate when the vehicle speed is constant or mildly changing. This means that the filter can be improved again, leading to the implementation of Kalman Filter #3.

7.3.3 Kalman Filter #3

The equations for Kalman Filter #3 are the same as those in Kalman Filter #2, given by Equations (7.8) – (7.12). The goal for this filter, though, is to improve the velocity estimation during Test 1. Test 1 is defined by slowly-changing velocity and slowly-changing acceleration, meaning the acceleration and jerk values during this time have a low magnitude. A clean jerk signal can be estimated by filtering the longitudinal acceleration and differentiating.

It was stated earlier that the low-cost GPS velocity measurement has a standard deviation of 0.5 m/s when the velocity is slowly changing, as in Test 1. Referring to Figure 7.10, the large error in the GPS velocity between the times of 70 and 80 seconds is caused by the GPS receiver losing a lock on satellites and the dilution of precision becoming very large. With this 10 second time segment as an exception, the GPS velocity is an accurate measurement for Test 1 (less than 0.5 m/s RMS). Currently, the velocity variance is set at a value of 1.7 m/s. So, it follows that the velocity variance value can be updated in the Kalman filter to better reflect these situations. Two different noise models will be used in Kalman Filter #3, depending on the level of acceleration and jerk excitation.

The GPS velocity error is plotted in Figure 7.33 for the two cases for the entire duration of Tests 1-3. The error for the first case (low jerk and acceleration) is significantly less than the error for the second case. This plot supports the reasoning to modify the Kalman filter to include different values of error characteristics depending on the current driving situation.

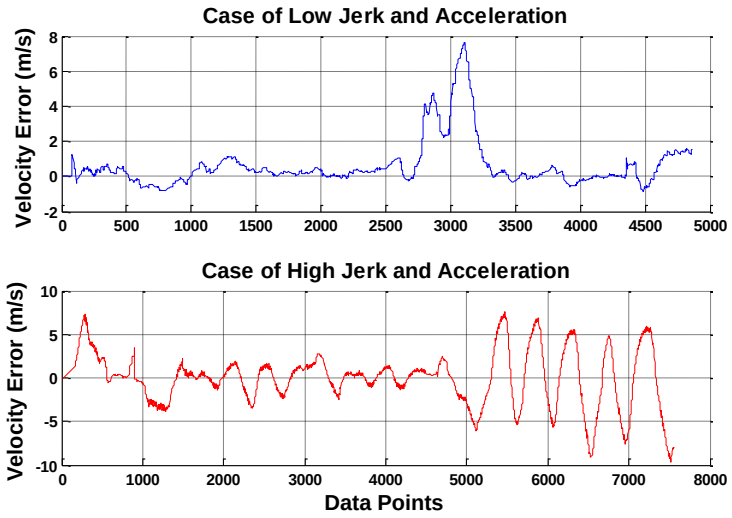

Figure 7.33. Velocity errors for the two cases of jerk and acceleration magnitudes during Tests 1-3

For time intervals when the jerk magnitude is less than 0.2 m/s^3 and the acceleration magnitude is less than 1.0 m/s^2, the standard deviation of the velocity error is changed to 0.5 m/s from 1.7 m/s. At the same time, the accelerometer standard deviation is increased from 0.5 m/s^2 to 2.5 m/s^2. The purpose of this change is to make the Kalman filter rely more on the GPS velocity measurement during this time. So, the standard deviation values to be used by Equations (7.11) and (7.12) for Kalman Filter #3 are outlined in Table 7.5. The values for the first case of jerk magnitude greater than 0.2 m/s^3 and acceleration magnitude greater than 1.0 m/s^2 are the same values as those used by Kalman Filter #2.

Table 7.5. Standard deviations used in Kalman Filter #3

Case	**|Jerk| > 0.2 m/s^3** **|Acceleration| > 1.0 m/s^2**	**|Jerk| ≤ 0.2 m/s^3** **|Acceleration| ≤ 1.0 m/s^2**
Velocity Std Dev (σ_v)	1.7 m/s	0.5 m/s
Acceleration Std Dev (σ_a)	0.5 m/s^2	2.5 m/s^2

The results are now presented for Kalman Filter #3 in Figure 7.34 through Figure 7.42. Table 7.6 displays the RMS velocity error for Kalman Filter #3.

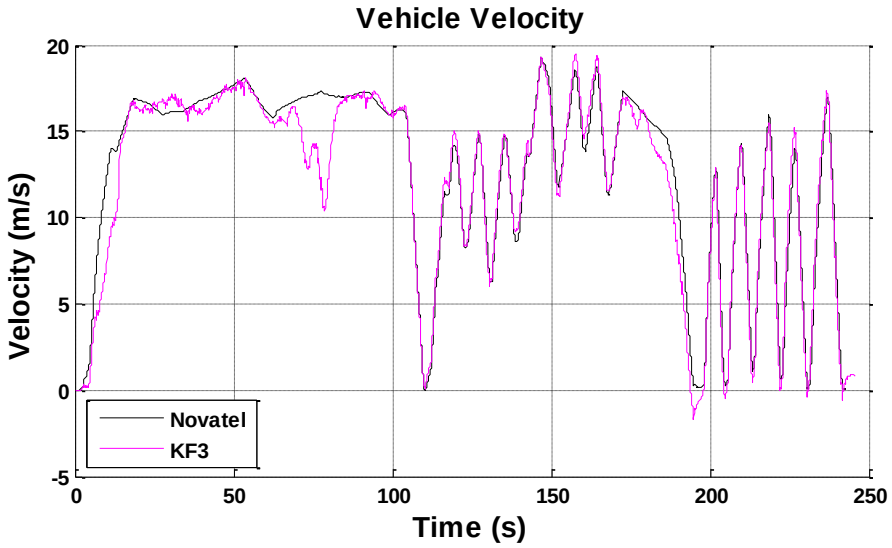

Figure 7.34. Velocity estimate from Kalman Filter #3

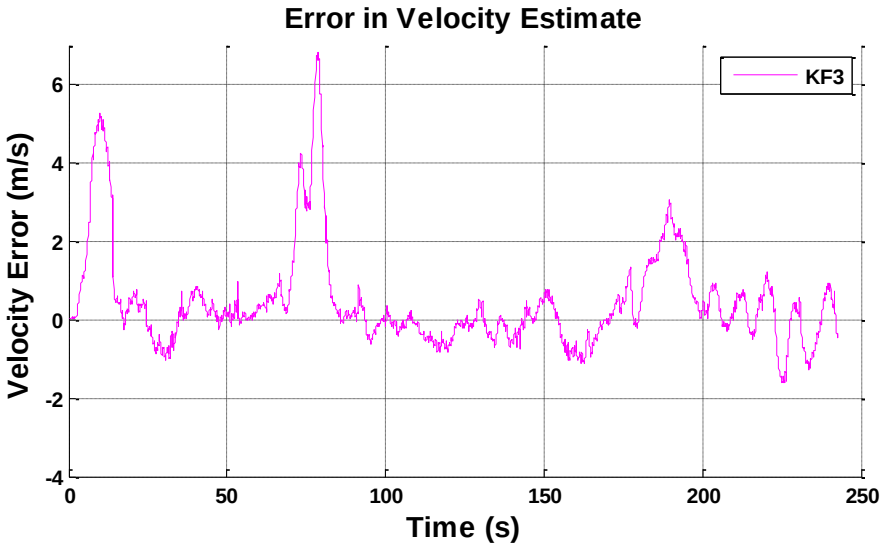

Figure 7.35. Error in velocity estimate from Kalman Filter #3

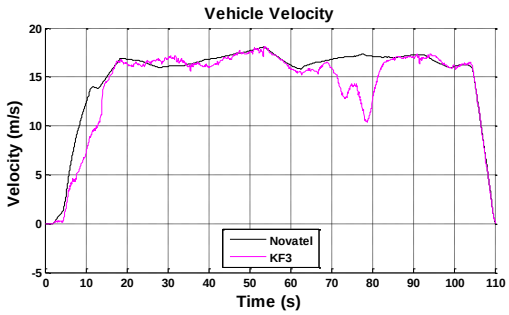

Figure 7.36. Velocity estimate from Kalman Filter #3 for Test 1

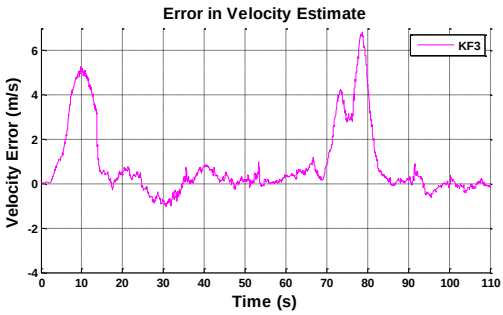

Figure 7.39. Error in velocity estimate from Kalman Filter #3 for Test 1

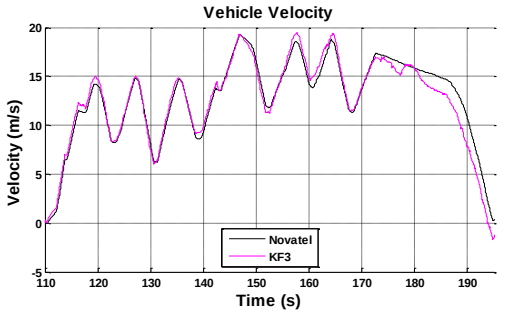

Figure 7.37. Velocity estimate from Kalman Filter #3 for Test 2

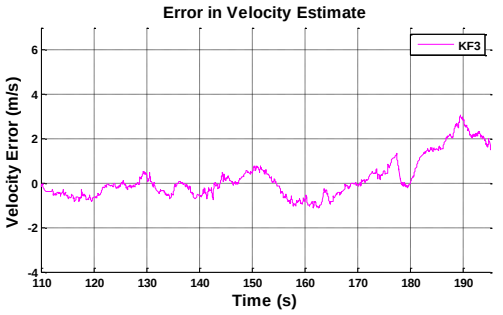

Figure 7.40. Error in velocity estimate from Kalman Filter #3 for Test 2

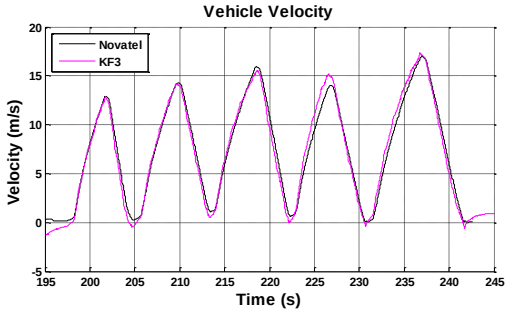

Figure 7.38. Velocity estimate from Kalman Filter #3 for Test 3

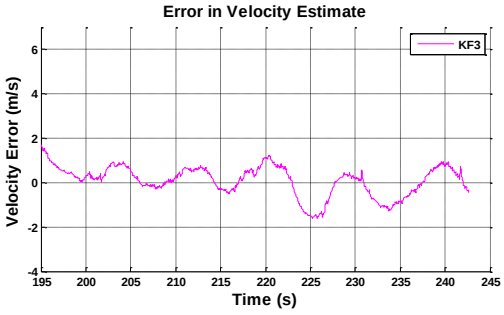

Figure 7.41. Error in velocity estimate from Kalman Filter #3 for Test 3

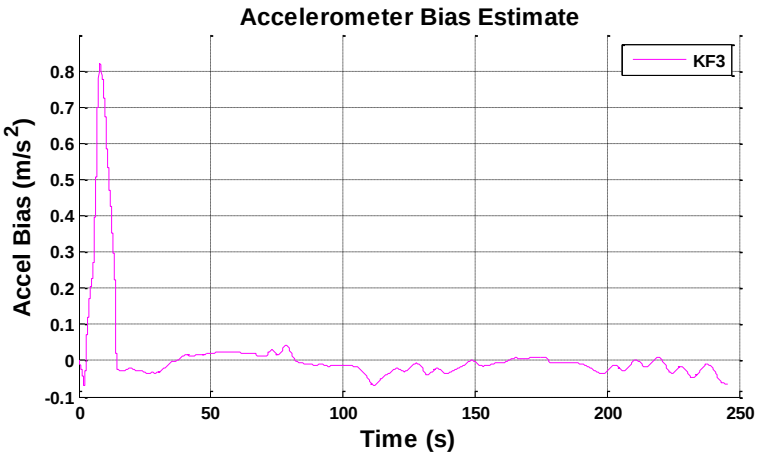

Figure 7.42. Accelerometer bias estimate from Kalman Filter #3

Table 7.6. RMS velocity errors for Kalman Filter #3

	Overall	**Test 1**	**Test 2**	**Test 3**
RMS Velocity Error (m/s)	1.3575	1.7879	0.9308	0.6742

This filter has the best overall performance with regards to RMS error, but also outperforms the raw GPS receiver and the other filters for each individual test. The velocity error for Test 3 is reduced by more than 85% over the raw GPS velocity for this test. This Kalman filter trusts the GPS velocity measurement when the vehicle speed is constant or slowly-changing, and trusts the accelerometer during dynamic driving conditions. It fuses the measurements to provide an optimal estimate of the vehicle velocity, reducing the velocity error by 50% over the raw GPS – from 2.76 m/s RMS to 1.3575 m/s RMS overall. However, it is still unknown whether the improvement over the raw GPS measurement due to this Kalman filter is enough to rely on the velocity estimate in a collision warning algorithm. The following chapter will address this issue.

Chapter 8

Meta-Analysis of Results

This chapter provides a summary and system-level analysis of the results from the previous chapters of this thesis. The Kalman filter implementation for the proposed system greatly increases the performance, but this chapter will examine whether the improvement is enough to satisfy accuracy requirements for successful collision warning.

8.1 Summary of Kalman Filtering Results

The velocity profiles and corresponding errors for the GPS receiver and three Kalman filters are given in the following plots, Figure 8.1 through Figure 8.8. Table 8.1 provides a summary of the RMS error values for each of the filters. It can be seen that employing a Kalman filter for the proposed collision warning system is very beneficial.

Table 8.1. RMS velocity errors for the GPS and all Kalman filters

	Overall	**Test 1**	**Test 2**	**Test 3**
Raw GPS	2.76	1.9753	1.6369	4.9919
Kalman Filter #1	1.5031	1.7872	1.3161	1.0179
Kalman Filter #2	1.7608	2.3678	1.1209	0.7737
Kalman Filter #3	1.3575	1.7879	0.9308	0.6742

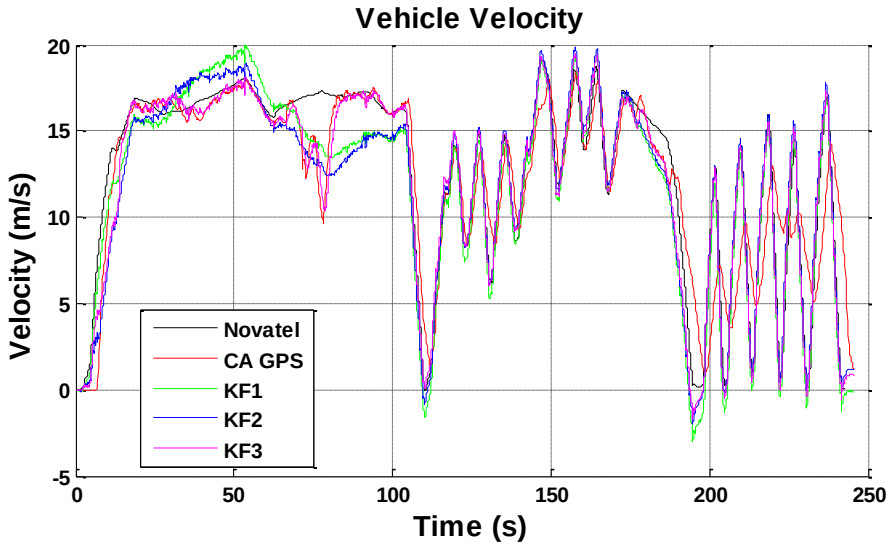

Figure 8.1. Velocity profiles from the GPS and all Kalman filters

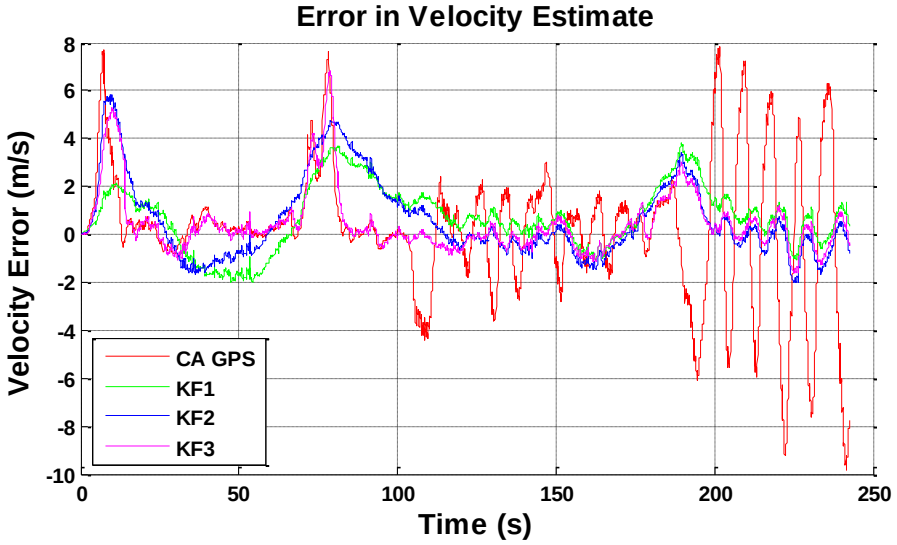

Figure 8.2. Errors in the velocity profiles from the GPS and all Kalman filters

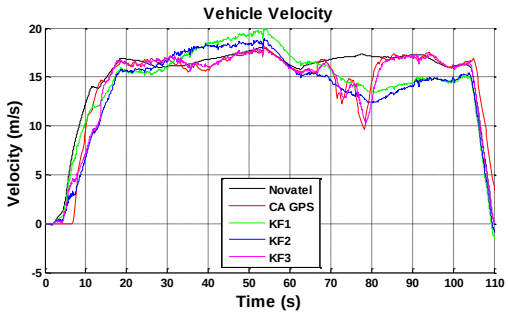

Figure 8.3. Velocity profiles from the GPS and all Kalman filters for Test 1

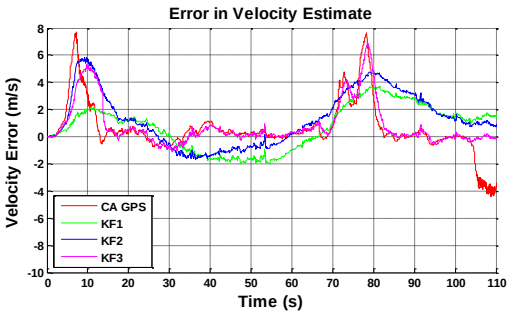

Figure 8.6. Errors in the velocity profiles from the GPS and all Kalman filters for Test 1

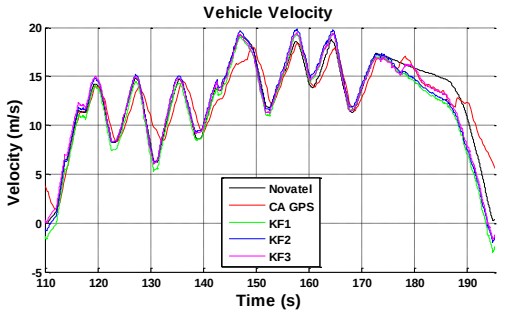

Figure 8.4. Velocity profiles from the GPS and all Kalman filters for Test 2

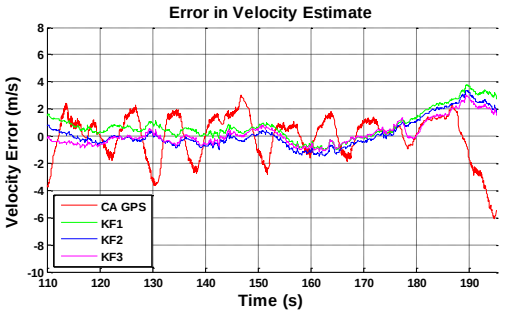

Figure 8.7. Errors in the velocity profiles from the GPS and all Kalman filters for Test 2

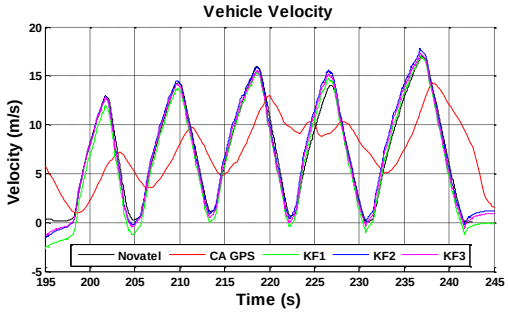

Figure 8.5. Velocity profiles from the GPS and all Kalman filters for Test 3

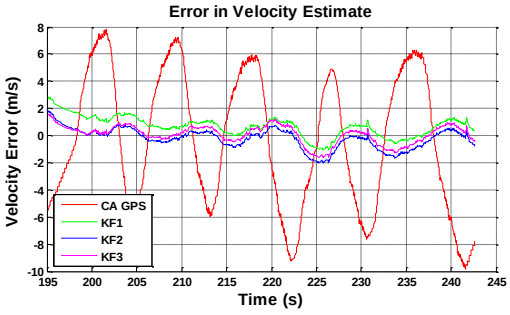

Figure 8.8. Errors in the velocity profiles from the GPS and all Kalman filters for Test 3

The Kalman filter implementation in this thesis is focused on reducing the error in the velocity estimate for the vehicle. Accurate velocity estimation is essential to the performance of the proposed collision warning system, as the velocity estimate directly relates to two of the collision warning algorithm's inputs – host velocity and relative velocity. Also, it is imperative that the collision warning system performs well in situations when collisions are most probable. These situations are generally characterized by sudden braking maneuvers and quickly-changing speeds, meaning that the accuracy of the velocity estimate is particularly important.

While it is clear that the implementation of Kalman Filter #3 yields RMS velocity errors that are much less than the raw measurement from the low-cost GPS receiver, there is currently no metric for determining whether the resulting velocity estimates are "good enough" to use in the collision warning algorithm. This issue is addressed in the following section.

8.2 Sensitivity Analysis to find Velocity Requirements

Previous research has quantified accuracy requirements on the headway distance measurement and timeliness of warnings issued by a collision detection system [**5**], [**10**]. Stated previously and shown in Table 2.1, Kamiya, et al. determined that the headway distance calculation should be within an error of 1 m, and the warnings should update at 0.1 s [**5**]. Shladover and Tan give similar requirements, stating that the desirable error on the headway distance measurement should be less than 0.7 m and the system should predict TTC to within 0.2 s [**10**]. But, there is no such requirement outlined for the velocity measurement.

To obtain an equivalent requirement, a simple sensitivity analysis was performed on the collision warning algorithm to determine the relationship between the distance and time requirements to the velocity estimate. The warning parameter is given in Equation (4.2) and can be written as

$$w = func(d, v, v_{rel}, \alpha, \tau, d_0) \tag{8.1}$$

Assuming first-order effects dominate, the sensitivity of the warning parameter to errors in each of the variables is given by the chain rule:

$$\Delta WP = \frac{\partial WP}{\partial d}\Delta d + \frac{\partial WP}{\partial v}\Delta v + \cdots + \frac{\partial WP}{\partial d_0}\Delta d_0 \tag{8.2}$$

By substituting the Δd and $\Delta \tau$ components with the error requirements mentioned above and allowing the other Δ terms to equal zero, the sensitivity of the warning parameter (ΔWP) can be found for each metric. Using Equation (8.2), the equivalent velocity error requirement (Δv) can be derived using the resulting known ΔWP.

This procedure was performed for each of the four metrics (Δd = 1 m, Δd = 0.7 m, $\Delta \tau$ = 0.1 s, $\Delta \tau$ = 0.2 s) using parameters that are representative of normal convoy driving situations, outlined in Table 8.2. The values of the tunable parameters – namely α, τ, and d_0 – are the same values that were used during the field testing presented throughout this thesis. The headway distance was chosen to be 20 m, as this was a commonly-seen following distance exhibited during field testing. (The headway distance actually has no bearing on the equivalent velocity error, as its effect is negated with the warning parameter value when the sensitivity is performed.) A relative velocity of 5 m/s was chosen to in order to simulate a situation where the preceding vehicle is braking.

The velocity is varied between 5 and 30 m/s to examine the effect of vehicle speed on the resulting equivalent velocity error.

Table 8.2. Parameters used for the sensitivity analysis of the warning parameter

Parameter	Value
Headway Distance, d	20 m
Velocity, v	5-30 m/s
Relative Velocity, v_{rel}	5 m/s
Maximum Deceleration, α	8 m/s^2
Time Delay, τ	1.4 s
Distance Buffer, d_0	5 m

The equivalent velocity error requirements are plotted in Figure 8.9 for the range of velocities examined. Note that the velocity error requirement relaxes as the host vehicle speed increases, an observation that was also noted in [**10**]. However, the severity of the warning parameter increases (the warning parameter value decreases) as vehicle speed increases, e.g. the faster a convoy is moving, the more important it is to have an accurate velocity measurement. At a velocity of 10 m/s, the warning parameter value is 0.83 for these conditions. At 15 m/s, it is 0.59, and at 20 m/s it is 0.45.

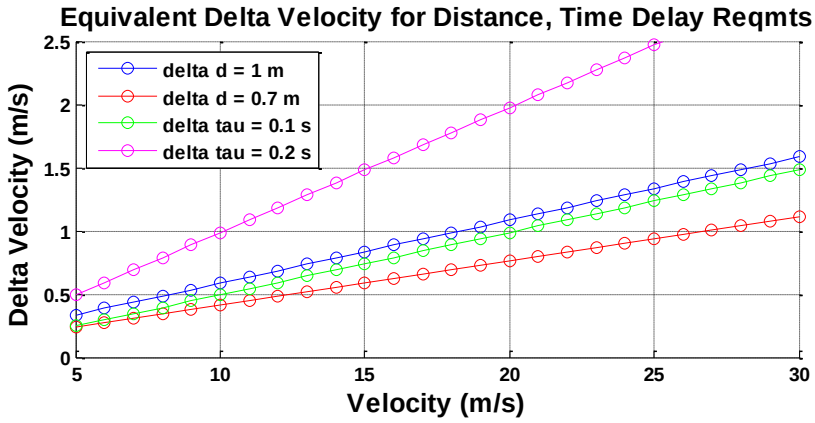

Figure 8.9. The equivalent velocity error derived from the distance and time delay specifications for a collision detection algorithm

It was stated earlier in the chapter that the performance of the collision warning system should be best when rear-end collision are most probable. These situations are generally characterized by high accelerations and decelerations (like sudden braking events in a convoy). Hence, these are situations when the warning parameter will indicate that a collision avoidance maneuver is needed – either a braking or steering action. So, with this logic, it is reasonable to assume that appropriate metric on the velocity estimate error can be taken from Figure 8.9 when the vehicle velocity was 15 m/s (and the warning parameter was 0.59). Vehicle speeds greater than 15 m/s give more a more relaxed error requirement, and vehicle speeds less than 15 m/s are associated with a milder warning parameter value.

From Figure 8.9 and the sensitivity analysis, the velocity error metric is taken to be within the range of 0.5844 m/s to 1.4815 m/s. The velocity error metric falls within a range because it depends on the original distance or time metric from which it is derived. This range can be used to quantify the performance of the Kalman filters for the proposed collision warning system. The velocity estimate from Kalman Filter #3 satisfies the requirement outlined by this range of error values. The velocity estimate from Tests 2 and 3 – the tests defined by speed variations and high

accelerations – show that the performance is also sufficient for the proposed system to be feasible to match the equivalent performance requirements given by other researchers.

8.3 Performance vs. Cost Tradeoff

The original goal of this thesis was to provide a low-cost, easily-incorporated collision warning system for military vehicle convoys. Considering this goal, it is important to classify the performance of the proposed collision warning system with cost in mind. The Novatel SPAN system provides velocity measurements (that were taken as truth for this study) that are accurate to within only a few centimeters per second. Yet, its effective cost for this study is around $10,000. Gupta developed a low-cost GPS/IMU system able to provide velocity readings within 0.3 m/s for near $600 (estimated) [**32**]. The sensor suite for the prototype system developed for this work costs about $200 and has an associated RMS velocity error that is less than 1 m/s when the vehicle's speed is moderately changing.

Figure 8.10 below summarizes the performance vs. cost tradeoff for forward velocity measurements during Test 3. The error bounds shown in the plot correspond to the range of velocity error metrics derived from the distance and time error metrics necessary for a collision warning system. Integrating the MEMS accelerometer with the low-cost GPS unit greatly increased the accuracy of the velocity measurement from the prototype system for only a slight increase in cost over the GPS receiver alone. To continue to reduce the velocity error, a much higher cost is required, evidenced by the GPS/IMU from Gupta and the Novatel SPAN system. Hence, the selection of the sensor suite for the work in this thesis is validated by its adequacy in performance with respect to its low cost.

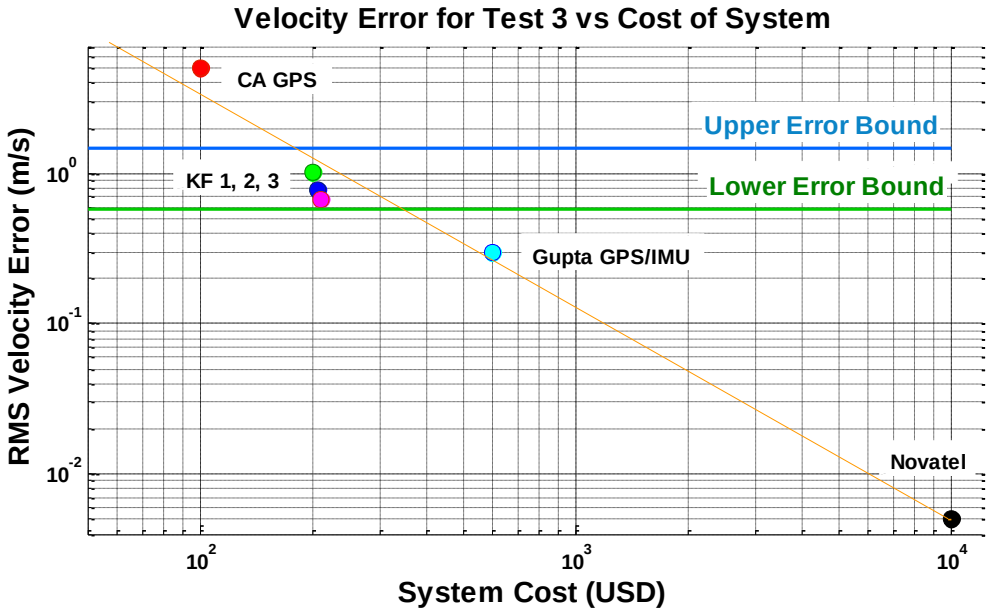

Figure 8.10. Plot of the Test 3 RMS velocity error from a system vs. the system cost

Despite the lack of analytical equations, the plot above suggests that there is a logarithmic relationship between sensor performance and cost. The orange line represents the approximate trend and can be used in the future to roughly estimate the performance-cost tradeoff of a sensor. From the trend, a velocity sensor with errors less than 1 m/s costs hundreds of dollars. A velocity sensor with errors less than 0.1 m/s costs thousands of dollars, and so on. The relationship presented in this plot can be a useful tool for future research.

Chapter 9

Conclusions and Future Work

It was stated in the Introduction that the main goal of this thesis was to provide a framework for a low-cost, easily-incorporated collision warning system to be used in military vehicle convoys. Most existing commercially-available collision detection systems are radar-based systems that are expensive and restricted by inherent limitations of radar. These limitations are, most significantly, degraded performance in adverse weather, restriction to line-of-sight driving situations, and inability to distinguish roadside obstacles from preceding vehicles in the path of travel. Thus, a GPS-based collision warning system was proposed. By transmitting vehicle positions and velocities over a wireless vehicle network, the proposed system is capable of improved performance over radar-based systems in the areas where radar is limited.

The proposed GPS-based collision warning system consists of only a few components: a sensor suite that includes a GPS receiver and MEMS accelerometer, a computer, a wireless vehicle network access point, and a driver display. This proposed system is cheaper than existing radar systems and can be easily incorporated into existing convoy vehicles.

A prototype collision warning system was developed to perform the field testing presented throughout this thesis. Initial testing of the prototype system showed that the proposed collision warning system is feasible, as the prototype system provided warnings of unsafe situations before

the drivers recognized for themselves that the situations were unsafe. Initial field tests at Yuma Proving Grounds showed that the concept for the proposed system works in dusty environments – a necessity for any military collision warning system. The prototype system experienced no degraded performance even when the dust from preceding convoy vehicles completely blocked the field of view.

The performance of the prototype collision warning system was drastically improved by fusing the GPS velocity measurement with the longitudinal acceleration reading from the MEMS accelerometer. By applying a discrete time Kalman filter, the velocity estimate error for the prototype system was reduced by 50% over the raw GPS velocity measurement. In driving situations where rear-end collisions are most probable, specifically those situations characterized by extreme decelerations, the Kalman filter improved the velocity estimate by more than 85% to an RMS error of 0.6742 m/s.

The Kalman-filtered velocity estimate satisfies the required velocity accuracy for successful collision detection and warning. Metrics for the velocity accuracy were derived from headway distance requirements and requirements on the timeliness of collision warnings. Without the Kalman filtering, the low-cost GPS-based collision warning system fails to meet performance requirements outlined by previous researchers. With the Kalman filtering, the proposed system is both feasible and realizable for successful rear-end collision warning within vehicle convoys.

9.1 Future Work

The future work that is listed below stems from extensions to the work that is presented in this thesis.

Determination of Algorithm Parameters

Presented below in Table 9.1 is a confusion matrix for the braking events plotted in Figure 5.19. For the tests represented here, warning parameter values greater than 0.8 designate situations that were deemed safe by the collision warning algorithm. Warnings less than 0.4 designate predicted collisions. Warnings between these values represent situations where the following vehicle is predicted to breach the distance buffer but not collide.

From the table below, the conservative nature of the collision warning algorithm used by the prototype system is evident. A completely diagonal matrix would represent a "perfect" collision warning algorithm. This matrix shows that safe stop events occurred even when the warning parameter predicted a collision. There are no results that display a non-conservative algorithm behavior where a breach or collision occurred that was not predicted.

Table 9.1. Confusion matrix of predicted outcome of braking events vs. actual outcomes

		Actual Result of Braking Event		
Predicted Result	**Warning Parameter Value**	**Safe Stop**	**Breached 5m Buffer**	**Collision**
	$WP > 0.8$	8	0	0
	$0.8 > WP > 0.4$	5	3	0
	$0.4 > WP$	1	2	4

The results of this table prove that there is much research that can be done on determining the parameter values to use in the collision warning algorithm. A diagonal matrix means that the collision warning algorithm is always correct in predicting collisions. So, by researching parameter values like the time delay, the range of values that govern a conservative vs. non-conservative system can be determined, and the collision warning algorithm can be tuned appropriately.

LIDAR Testing for Headway Distance Evaluation

It was stated earlier that GPS position measurement errors are correlated spatially and temporally. To verify this claim and assess the accuracy of the headway distance calculation from the prototype system, LIDAR tests should be performed to obtain a ground truth measurement of the headway distance in a two-vehicle convoy.

Expansion of Kalman Filter to 2D

The complexity of the Kalman filter can be expanded to include 2D state estimation. The north and east positions and velocities can be estimated using the heading measurement from the GPS. GPS position and velocity readings can be used for the Kalman filter update and lateral and longitudinal accelerations for the predictions. By collecting the DOP from the GPS receiver (or even each satellite location), the Kalman filter can better model the noise from the receiver.

Road Grade Estimation using GPS

It seems from the field testing results that the acceleration measurements are affected by vehicle pitch and road grade. The altitude and vertical velocity measurements from the GPS receiver should be collected to get an estimate of the current road grade. Including this estimate in the Kalman filter can improve the other state estimates.

Mobile DGPS Implementation within the Convoy

The specific nature of the proposed system and the assumption that it will be used with vehicle convoys opens avenues for researching methods to utilize differential GPS corrections in the proposed collision warning system. A DGPS receiver or beacon receiver can be installed on one of the convoy vehicles. The DGPS corrections received by this receiver can be broadcast over the wireless network to the rest of the convoy vehicles. This way, all vehicles in the convoy can receive differential corrections without actually being equipped with a differential receiver.

Also, there can be research done on the ways to use the GPS receivers in the convoy to do some sort of "moving DGPS" implementation. This idea is based on the concept of a roving base station that knows its position by using the assumption that all convoy vehicles are traversing the same path.

Learning the Convoy Vehicle Ordering

Algorithms should be researched that use the GPS position, velocity, and heading to learn the ordering of the convoy vehicles. The collision warning algorithm relies on the information from two consecutive vehicles, so the ordering of vehicles is important.

Collection of DOP from GPS Receiver

The dilution of precision reported by the low-cost GPS receiver should be collected and used for the DOP value in the Kalman filter. Inputting the actual value of DOP will alleviate much of the error in the Kalman filter caused by the loss of GPS lock.

Bibliography

[1] J. D. Lee, D. V. McGehee, T. L. Brown, and M. L. Reyes, "Driver distraction, warning algorithm parameters, and driver response to imminent rear-end collisions in a high-fidelity driving simulator," US Department of Transportation NHTSA, 2002.

[2] Eaton VORAD, "The Benefit of Collision Warning Systems for Commercial Vehicles," in *ITS America Annual Meeting*, 2001.

[3] A. Doi, et al., "Development of a rear-end collision avoidance system with automatic brake control," *JSAE Review*, vol. 15, pp. 335-340, Feb. 1994.

[4] A. Nmngani and M. Akyurt, "A Review of Vehicle Collision Avoidance Systems," in *Saudi Engineering Conference*, Dhahran, 2002, pp. 413-428.

[5] H. Kamiya, et al., "Intelligent Technologies of Honda ASV," Honda R&D Co., Ltd., 1996.

[6] Y. Fujita, K. Akuzawa, and M. Sato, "Radar Brake System," *1995 Annual Meeting of ITS America*, vol. 1, pp. 95-101, Mar. 1995.

[7] P. Seiler, B. Song, and J. K. Hedrick, "Development of a Collision Avoidance System," University of California-Berkeley SAE Publication 98PC-417, 1998.

[8] K. Lee and H. Peng, "Evaluation of automotive forward collision warning and collision avoidance algorithms," *Vehicle System Dynamics*, vol. 43, no. 10, pp. 735-751, Oct. 2005.

[9] E. R. Hoffmann and R. G. Mortimer, "Drivers' Estimates of Time to Collision," *Accident Analysis and Prevention*, vol. 26, no. 4, pp. 511-520, 1994.

[10] S. E. Shladover and S.-K. Tan, "Analysis of Vehicle Positioning Accuracy Requirements for Communication-Based Cooperative Collision Warning," *Journal of Intelligent Transportation Systems*, vol. 10, no. 3, pp. 131-140, 2006.

[11] Eaton Corporation, "VORAD Collision Warning System for Military Vehicles," Brochure, 2007.

[12] Delphi Corporation, "Delphi Safety & Security Systems," Brochure, 2005.

[13] Meritor WABCO Vehicle Control Systems, "OnGuard Collision Safety Systems," Brochure, 2008.

[14] Mobileye Technologies Limited, "Mobileye AWS-4000," Brochure, 2007.

[15] Siemens VDO Automotive AG, "pro.pilot Advanced Driver Assistance Systems for Commercial Vehicles," Brochure, 2007.

[16] Eaton Corporation, "VORAD VS-400 System Packages," Brochure, 2008.

[17] Battelle, "Phase II Driver Survey Report: Volvo Intelligent Vehicle Initiative Field Operational Test," US Department of Transportation, Washington, D.C., Final Report, 2004.

[18] P. Davies, *Assessment of Advanced Technologies for Relieving Urban Traffic Congestion*. Washington, D.C., USA: NCHRP Transportation Research Board, 1991.

[19] NIMA, "Department of Defense World Geodetic System 1984," National Imagery and Mapping Agency TR8350.2, 1997.

[20] P. Misra and P. Enge, *Global Positioning System: Signals, Measurments, and Performance*, Second Edition ed. Lincoln, MA, USA: Ganga-Jamuna Press, 2006.

[21] W. Chen and S. Cai, "Ad Hoc Peer-to-Peer Network Architecture for Vehicle Safety Communications," *IEEE Communications Magazine*, pp. 100-107, Apr. 2005.

[22] M. Preuss and S. Thomas, "Wireless, Mesh & Ad Hoc Networks: Military Convoy Location and Situation Awareness," US Army CERDEC.

[23] R. W. Sinnott, "Virtues of the Haversine," *Sky and Telescope*, vol. 68, no. 2, p. 158, 1984.

[24] A. Boukerche, H. A. B. F. Oliveira, E. F. Nakamura, and A. A. F. Loureiro, "Vehicular Ad Hoc Networks: A New Challenge for Localization-Based Systems," *Computer Communications*, vol. 31, pp. 2838-2849, 2008.

[25] D. Simon, *Optimal State Estimation*. Hoboken, NJ, USA: John Wiley & Sons, Inc., 2006.

[26] Y. Bar-Shalom, X. R. Li, and T. Kirubarajan, *Estimation with Applications to Tracking and Navigation*. New York, USA: John Wiley & Sons, Inc., 2001.

[27] R. F. Stengel, *Optimal Control and Estimation*. New York, USA: Dover Publications, Inc., 1994.

[28] D. M. Bevly, "Global Positioning System (GPS): A Low-Cost Velocity Sensor for Correcting Inertial Sensor Errors on Ground Vehicles," *Journal of Dynamic Systems, Measurement, and Control*, vol. 126, pp. 255-264, Jun. 2004.

[29] D. M. Bevly, J. C. Gerdes, C. Wilson, and G. Zhang, "The Use of GPS Based Velocity Measurements for Improved Vehicle State Estimation," in *American Control Conference*, Chicago, 2000, pp. 2538-2542.

[30] S. Rezaei and R. Sengupta, "Kalman Filter-Based Integration of DGPS and Vehicle Sensors for Localization," *IEEE Transactions on Control Systems Technology*, vol. 15, no. 6, pp. 1080-1088, Nov. 2007.

[31] J. Ryu and J. C. Gerdes, "Integrating Inertial Sensors With Global Positioning System (GPS) for Vehicle Dynamics Control," *Journal of Dynamic Systems, Measurement, and Control*, vol. 126, pp. 243-254, Jun. 2004.

[32] V. Gupta, "Vehicle Localization Using Low-Accuracy GPS, IMU and Map-Aided Vision," PhD Thesis, Penn State University, University Park, PA, 2009.

[33] D. W. Allan, "Statistics of Atomic Frequency Standards," in *Proceedings of the IEEE*, 1966, pp. 221-230.

[34] The Analytical Sciences Corporation, *Applied Optimal Estimation*, A. Gelb, Ed. Cambridge, MA, USA: The M.I.T. Press, 1989.

Appendix A

Photos of Testing at Yuma Proving Grounds

Appendix B

Sample MATLAB Code for Kalman Filtering

```
function xhat = run_kalman_filter(time,data)

% time  :   1: simulation time (s)

% data  :   1: GPS time (s)
%           2: GPS latitude (deg)
%           3: GPS longitude (deg)
%           4: GPS velocity (m/s)
%           5: GPS course (deg)
%           6: Accel X (m/s^2)

%% KALMAN FILTER
% velocity as measurement, and longitudinal acceleration as an input
% STATE VECTOR:  [  s   ]   distance traveled
%                [ sdot ]   velocity
%                [  bf  ]   accelerometer bias

%%

gpstime = data(1,:);
velocity = data(4,:);
acceleration = data(6,:);

xhat = zeros(3,length(time));

%%
%Time Step
dt = 0.02;      % seconds

Tcf = 1300;     % seconds
Sf = 0;
DOP = 2;

% State Equation
% xdot = Fx + Gu + Lw
F = [0 1 0; 0 0 -1/(1+Sf); 0 0 -(1/Tcf)];
```

```
G = [0; 1/(1+Sf); 0];
L = [0 0 0; 0 1 0; 0 0 1];

% Measurement Equation
% z = Hx + n
H = [0 1 0];

% System Dynamic Equation
% xk = Phik_1 * xk_1 + Gammak_1 * uk_1 + Lambdak_1 * wk_1
Phik = expm(F*dt);
% Gammak = (Phik - eye(2))*inv(F)*G;
% Lambdak = (Phik - eye(2))*inv(F)*L;
% Since F is singular...
Gammak = Phik*(eye(3) - (1/2)*F*dt + (1/6)*F^2*dt^2 -
(1/24)*F^3*dt^3)*G*dt;
Lambdak = Phik*(eye(3) - (1/2)*F*dt + (1/6)*F^2*dt^2 -
(1/24)*F^3*dt^3)*L*dt;

%Variances
sigma_dist = 5;     % distance
sigma_vel = 1.7;    % velocity
sigma_accel = 0.5;  % acceleration
sigma_bf = 0.01;    % bias

Qk_prime = [0 0 0; 0 sigma_accel^2 0; 0 0 sigma_bf^2];
Rk = sigma_vel^2*DOP;
Qk = Lambdak*Qk_prime*Lambdak';

%%
% Initial Conditions
xhatk_1 = [0; 0; 0];
Pk_1 = [1 0 0; 0 1 0; 0 0 1];
uk_1 = 0;
zk_1 = 0;
gpstk_1 = 0;

% Since we have constant matrices...
Phik_1 = Phik;
Gammak_1 = Gammak;
Lambdak_1 = Lambdak;
Qk_1 = Qk;

%% KALMAN FILTER LOOP

for i = 1:length(time)
    gpstk = gpstime(i);
    zk = velocity(i);
    uk = acceleration(i);

    % EXTRAPOLATION STEP
    xhatk = Phik_1*xhatk_1 + Gammak_1*uk_1;
    Pk = Phik_1*Pk_1*Phik_1' + Qk_1;
```

```
    % FILTER GAIN COMPUTATION
    Kk = Pk*H'*(H*Pk*H' + Rk)^(-1);

    % UPDATE STEP
    if gpstk ~= gpstk_1
        xhatk = xhatk + Kk*(zk - H*xhatk);
        Pk = (inv(Pk) + H'*inv(Rk)*H)^(-1);
    end

    xhatk_1 = xhatk;
    Pk_1 = Pk;
    uk_1 = uk;
    zk_1 = zk;
    gpstk_1 = gpstk;

    xhat(:,i) = xhatk;
end

return;
%%
```